Case Studies in Thermal Engineering 49 (2023) 103261

Contents lists available at ScienceDirect

Case Studies in Thermal Engineering

journal homepage: www.elsevier.com/locate/csite

Catalysis reaction influence on 3D tetra hybrid nanofluid flow via oil rig solar panel sheet: Case study towards oil extraction

Tanveer Sajid [a], Wasim Jamshed [a,*], Salem Algarni [b], Talal Alqahtani [b], Mohamed R. Eid [c,d], Kashif Irshad [e], Gilder Cieza Altamirano [f,g], Sayed M. El Din [h], Khadiga Wadi Nahar Tajer [i]

[a] Department of Mathematics, Capital University of Science and Technology (CUST), Islamabad, 44000, Pakistan
[b] Department of Mechanical Engineering, King Khalid University, Abha, 61413, Saudi Arabia
[c] Department of Mathematics, Faculty of Science, New Valley University, Al-Kharga, Al-Wadi Al-Gadid, 72511, Egypt
[d] Department of Mathematics, Faculty of Science, Northern Border University, Arar, 1321, Saudi Arabia
[e] Interdisciplinary Research Centre for Renewable Energy and Power System (IRC-REPS), Research Institute, King Fahd University of Petroleum and Minerals (KFUPM), Dhahran, 31261, Saudi Arabia
[f] Universidad Nacional Autónoma de Chota, Cajamarca, Peru
[g] Fizmako Research Group, Bogotá, Colombia
[h] Center of Research, Faculty of Engineering, Future University in Egypt, New Cairo, 11835, Egypt
[i] Department of Mathematics, College of Science and Arts, Qassim University, Ar Rass, 51452, Saudi Arabia

GRAPHICAL ABSTRACT

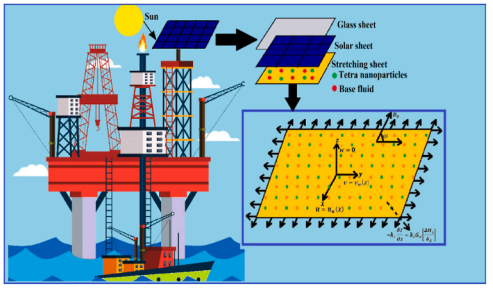

ARTICLE INFO

Handling Editor: Huihe Qiu

Keywords:
Tetra hybrid nanofluid (TETHNF)
Cubic autocatalysis

ABSTRACT

The power that comes from renewable sources is made back faster than it is used. Infinitely renewable examples include solar and wind energy. There are many sources of clean energy all around us.

* Corresponding author.
E-mail address: wasiktk@hotmail.com (W. Jamshed).

https://doi.org/10.1016/j.csite.2023.103261
Received 28 March 2023; Received in revised form 30 June 2023; Accepted 4 July 2023
Available online 7 July 2023

Inclined magnetic
Nanofluidics
Velocity slip
3D Cross fluid
Thermal conductivity

Motive behind current study: A framework has now been developed throughout this research to investigate the impact of the sun's rays on novel Xue tetra hybrid magnetized cross nano-liquid as it moves through an expanding sheet inside that PV sheet of a solar module installed on top of such an offshore solar oil field. A novel Xue tetra hybrid nanofluid model has been developed and utilized to explore the impact of tetrahybrid nanoparticles on liquid flowing in order to investigate heat transport analysis. By directing the liquid's motion through a magnetic field, we may examine its velocity impact. The concentration aspect of nanofluid has been examined by including homogeneous and heterogeneous chemical processes, and indeed, the temperature accessibility of cross-nanofluid is obtained by taking into consideration effects like thermal conductivity and thermal radiation.
Technique: The PDEs derived from the working prototype are then subjected to the resemblance factors, yielding the ODEs. The bvp4c scheme is used to get numerical results. The procedure is an ODE solver that belongs to the Runge-Kutta family. In order to provide precise answers in the fourth and fifth orders, it performs six function evaluations. The discrepancy between them is therefore interpreted as the solution's (fourth-order) inaccuracy. Adaptive stepsize integration techniques greatly benefit from this error estimation. Fehlberg's (RKF) integration strategy is quite similar to Cash and Carp technique.
Significant finding: From obtained results, it is detected that the addition of novel tetrahybrid nanoparticles in the conventional liquid (Xue tetrahybrid nanofluid) enhances heat transfer rate and temperature profile more quickly in contrast to conventional ternary hybrid nanofluid and dihybrid nanofluid available in the existing literature. The thing which makes the present work novel and one step ahead in contrast to existing available literature is the development and implementation of a tetrahybrid nanofluid model in contrast to conventional ternary hybrid and dihybrid nanofluid models. Tetra hybridity nanoliquid generates extra heat in distinction to already existing ternary hybridity and dihybrid nanofluid models and more heat is absorbed by PV sheets in the existence of tetrahybrid nanoparticles.
Conclusions: When the nanomaterials are submerged inside this liquid, their temperature increases throughout both the shear thinning and shear thickening cases. This is because the homogeneous chemical reaction mimics the migration of nanoparticles within the liquid. The increased magnetic force, in addition to an enhancement of Lorentz's force, slows down the nanofluid motion. The increased volume percentage of tetrahybrid nanoparticles, thermal radiation, and thermal conductivity boost the heat that's captured by a PV sheet, and that heat is utilized for other functions, such as drilling or navigation, on that solar offshore rig.
Cost analysis: Cost analysis has also been presented in terms of Pakistan offshore oil rigs in terms of solar panels and diesel generators and it is observed that 49% cost is reduced if we replaced offshore oil rigs with solar-powered energy.

1. Introduction

Non-Newtonian fluid has attracted the attention of scientists and investigators in the past few years as a result in its implementations in mechanical and industrial development. Shampoos, plasma, starch, cocoa, toothpaste, jelly, and pudding are all examples of non-Newtonian materials. The correlation between shearing stress and shearing rate differs in non-Newtonian substances. Consequently, a constant viscosity coefficient can't be considered. Although viscosity is often employed in the field of fluid mechanics to highlight the shear characteristics of a liquid, this property alone is not adequate to depict non-Newtonian fluids. Non-Newtonian fluids can only be shown by combining viscosity with other properties. They are best highlighted by a few extra rheological characteristics that relate stress and strain rate tensors under various flow limits, such as accretionary movement, and are calculated employing a variety of rheometers. This is the best way to emphasize them. Non-Newtonian processes may be broken down into three categories: shear-thinning, thickening, and dilatant substances. Rheology is the study of how the form of a fluid changes because of external forces being applied to it [1,2]. Rheology also refers to the study of how the shape of the fluid changes over time. Rheology may be used to inform a variety of different models. If the rate at which the deformation occurs is proportional to the shear rate, then the fluid is referred to as Newtonian fluid. On the other hand, if the deformation rate is nonlinear, then the fluid belongs to a different category and is referred to as non-Newtonian fluid. There are a number of nonlinear mathematical models that may be used to explain the behavior of fluids; however, there was no such specified model to examine the properties of fluids subjected to very high and extremely low shear rates until Carreau [3] published the Carreau Model. This was because of the complexity of the problem. This model has the competent property to deal with very low and high shear rates and deformation. Many scholars [4–13] did their investigations regarding Carreau fluid with different facts. Hosseinzadeh et al. [14] made Carreau fluid flow including motile gyrotactic micro-organisms and nanomolecules via a three-dimensional cylinder. Computational reproduction of heat transmission in MHD stagnating point flowing of Carreau fluid kind on a stretchable plate is explored by Hayat et al. [15]. Waqas et al. [16] depicted the nanofluid model and numerical outcome related to the stagnation region of Carreau fluid by expanding-contracting cylinder geometry. Theoretical aspects of thermophoresis and Brownian motion with three-dimensional Carreau fluid are numerically obtained by Sultan et al. [17]. For every Prandtl number, Shaw et al. [18] reported their study of magnetohydrodynamic flow and thermal interpretation of Carreau hybridity nanoliquid impacted by linear, non-linear, and quadratic thermal radionuclides.

There is certainly a lot of research going on about how to make modern nanofluids. These liquids were also assumed to somehow be ternary nanofluids (THNF). THNFs are better at transferring heat as multiple of their parts are linked together. This has a cumulative effect on the entire structure. Investigators across the entire world looked into THNF because it moves to heat more quickly than other hybrid nanofluids. Adun et al. [19] looked into different parts of THNFs and how they affect fluids. Sneha et al. [20] looked into the consequences of ternary HNF on a thermally coupled stress liquid moving through a permeable material with a convective boundary. Goud et al. [21] looked at how the THNF moves within the dovetail fin only when thermal conductivity changes. Nasir et al. [22] explored the impact of THNF on a magnetized liquid. Cao et al. [23] look at mixed convective THNF with radiation but also surface slip. Mahmood et al. [24] looked into the impact of the stagnation point on a magnetized THNF moving towards a cylinder with a heat source. Krishna et al. [25] looked into how THNF affects biomagnetic liquid even though it flows towards a wedge. They also used the MANFIS technique to address the conceptual model. Sajid et al. [26] looked at how THNF, chemical processes, and activation energy affected nanofluids moving in a wedge. Sajid et al. [27] looked into the consequences of THNF on cross-liquid. They took into account things like heat source and sink, but also heat flux. Sajid et al. [28] looked into how the Cattaneo-Christov heat fluxing and a non-linearly kind of heat supplier affect a tetra-hybrid Reiner-Philippoff liquid transport under a bendable sheet. Acharya [29] investigated the influence of a magnetism force on buoyancy-driven Ag–MgO-water hybrid nanofluidic flow within a cubical chamber with a circular cylinder fitted within it. Similar work on nanofluid in reported in Refs. [30–32].

The heat and MHD flows are affected by radioactivity at very extreme temperatures. So, it is crucial to comprehend the propagation of radiation emitted in order to create technological tools. A thorough understanding of heat radiative flux as well as mass transfer is required for the design of airplanes, turbines, spaceships, space vehicles, hydroelectricity, and countless agricultural applications. The term "thermal radiation" (TR) is used to describe the electromagnetic energy given off by a material according to its temperature. TR may be seen in the infrared light given out by the average radiator or heat exchanger used inside. Heat conduction via HNFs across porous materials was reviewed by Xu et al. [33]. Wakifet al. [34] researched the heat transfer durability of HNFs using copper and aluminum oxides as well as the TR features. Chen et al. [35] inspected how combining HNFs involved NFs' TR holdings. The flow of HNFs was controlled by Agrawal et al. [36] using TR effects across an area of the porous medium that looked to somehow be thoroughly embedded. Using peristaltic motion, Prakash et al. [37] pumped magnetized HNFs exhibiting TR as well as heat-dependent viscosity properties. Khan et al. [38] used a FEM approach to generate magnetic dipoles as well as TR impacts on the stationary movement of micro-polarly developed NFs across a vastly increasing slip. The MHD impact on wedge movement of non-Newtonian NFs was analyzed by Ali et al. [39] in terms of TR and driving energy. The MHD motion of HNFs induced by various TRs was used by Shaw et al. [40]. The hydrothermal component of a magnetization Ag–MgO-water-based nanoliquid flow that was traveling within an octagonal hollow and circular cylinder was investigated by Acharya [41]. Acharya [42] did extensive research on the influence that natural convection has on magnetized generated Ag–MgO-water hybridity nanofluid flowing when the enclosure was circular and equipped with I-shaped rectangular fins of varying lengths. The flowing was exposed to the enclosure.

Different mechanisms in the environment and industries frequently see mass transit due to fluctuations in concentrations. Whether a chemical reaction is homogenous or heterogeneous determines its influence [43]. It is not conceivable for nature to provide clean water and air at the same time. It is conceivable for any outer item to be present naturally or that it has been mixed with air or water. Both scenarios are viable possibilities. When an outside mass is present in air or liquids, this might cause a chemical reaction to take place. The understanding of linked chemical processes may be improved using several chemical technologies, such as those used in the processing of food, the production of glassware or ceramics, and the synthesis of polymers. Much research has lately been reported on the influence of chemical processes on hybridity nanofluid flow, revealing the applicability of these nanofluids in a number of scientific disciplines and industrial fields [44]. Collision of two or more substances with each other, there may be the product of two or more produced materials, this process is termed as a chemical procedure. There are basically two types of chemical processes named homogeneous chemical reaction and heterogeneous chemical reaction. The reaction which happens in the mono phase is called a homogeneity chemical reaction and happens in a different phase called a heterogeneous chemical reaction. Another basic concept is the substance that helps to speed up the chemical reaction is called a catalyst, for example fire plays the role of the catalyst during tea. Three types of catalysts are positive, negative, or autocatalysis. The catalyst which speeds up is known as a positive catalyst while which decreases the rate of a chemical process is called a negative catalyst and the catalyst which does its work according to the situation is called an auto catalyst. These catalysts play a vital role in engineering, and everyday life like rubber for tires, medicine, fuel, and plastics. There are some processes in which catalysts are being utilized like zeolites, aluminum chloride, hydrogen chloride, nickel, platinum, or palladium, copper, oxide, vanadium oxide, platinum, and palladium. Many investigators made a bundle of numerical attempts regarding autocatalysis and chemical processes. Khan et al. [45] attained a numerical study related to MHD flow of viscous fluid with entropy generation analysis along the geometry of bent stretchable sheet with cubic autocatalysis chemically reactive flow. Further, a study [46] did work on cubic autocatalysis chemical reactive flow with entropy optimization with the addition of viscous dissipation. Ali et al. [47] published their exploration of thermal relaxation and cubic autocatalysis on a non-Newtonianism flowing range with MHD impacts. Thermal management and its analysis with a mathematical model of Carreau nanofluids over the geometry of a thin needle is discussed by Chu et al. [48].

1.1. Research gap

A lot of literature is available which investigates the effect of ternary and dihybrid nanofluids on liquid flowing exposed to diverse shapes like cone, cylinder, channel, needle, sheet, etc. This work is unique and original in the sense that no attention has been paid in existing literature and literature mentioned above to develop any nanofluid model comprises of tetra hybridity nanomolecules with ethylene glycol as a conventional liquid (Xue tetra hybrid nanofluid model) in order to study the effect of tetrahybrid nanofluid on cross fluid flow subjected to an expandable sheet.

1.2. Motive behind current research

Main purpose to launch this examination is to investigate the mathematical style of radiative non-Newtonian Cross nanoliquid associated with the inclined magnetized environment, cubic autocatalysis effect, tetrahybrid nanoparticles, and thermal conductivity. The temperature distribution is judged by temperature-dependent thermal conductivity and the concentration of nanofluid is being studied by incorporating homogeneous-heterogeneous chemical reactions. Heat transport and thermal relaxation flowing of Cross liquid are analyzed via heat diffusion under the impact of heat generating.

1.3. Novelty

Novel Xue tetrahybrid nanofluid has been developed and introduced in this article. This paper is innovative in the implication that the consequence of novel Xue tetrahybrid nanofluid on three-dimensional cross fluid with catalytic chemical reaction has not been researched yet in the existence literature. Moreover, computational analysis in terms of solar energy and diesel energy has been never debated before in the case of the offshore oil rig industry of Pakistan.

2. Solar energy use in offshore drilling

2.1. Working in offshore oil drilling

Oil firms identify the digging locations the more likely to yield oil employing sonic instrumentation. The first well is then dug using a mobile offshore digging unit (MODU). A few of the components are changed over to become operational rigs, which means that transition from searching and seeking oil to gathering it once it has been discovered. In order to collect oil, the oil firm will often substitute the MODU with an even more durable oil supply rig.

The listed below are the four primary categories of MODUs.

2.1.1. Submersible

In most cases, a submersible MODU has the appearance of a barge that is positioned somewhat on the bottom of the ocean. Steel stakes that rise well above the surface of the water may be found just on the platform of the barge. At the base of such steel, poles are where a digging station is located. Such rigs are frequently employed in regions that have rather peaceful water.

2.1.2. Jackup

An apparatus that has been mounted on the deck of something like a movable barge is known as a Jackup. The barge is towed to such a digging location by a boat. The feet of the Jackup may be extended towards the sea bottom after it has been installed. The feet are weighted that won't go through the floor surface when the chair is moved. After all the arms have been fastened in place, the Jackup will start to pull the legs upward in order to ensure the base will be elevated over the water. As a consequence, the rig is protected from the waves but also tidal movements. Jackups can work at depths that go as deep as 525 feet (160 m).

2.1.3. Drill ships

Ships that have been referred to as "bore ships" are equipped with drilling equipment mounted on the upper deck. The drill is activated via an opening in the hull of the vessel. Drilling boats are able to direct themselves toward the drilling location, and once there, they may utilize a mixture of anchors and rotors to compensate for any drift that may occur while the oil is being extracted using a rig. They can function in environments with deep water.

2.1.4. Semisubmersibles

Semisubmersibles float just on the water's surface above enormous, underwater boats. Propelling devices enable them to go to digging locations using their power whereas others need a secondary vehicle to pull it toward the proper position. In order to compensate for movement, computers manage the strain placed across each anchor chain. A few are able to transition from offshore drilling to operational rigs, meaning that if oil is discovered, there is less of a necessity to have an additional rig.

2.2. Power source to offshore oil rig

By far the most common way to get enough electricity to the rig is to use engines that are powered by regular diesel. Backup diesel generators that are located offshore, on the other hand, call for a different set of characteristics and settings. The circumstances are rough and unpredictable out at sea. Because of this, the turbines that have been manufactured to be utilized onboard oil rigs are required to be constructed using substances and varnishes that seem to be able to survive the temperature fluctuations, water, and even salinity that seem to be prevalent offshore, in addition to the wind. The cost of providing power to an offshore rig might be rather high. A diesel generator that powers an entire site in the world's largest oil and gas organization may use anywhere from 20 to 30 m3 of diesel per day. As a result of this, it is essential to seek out methods to lower the rig's energy usage yet guarantee it's as cost-effective as possible. Making sure that electricity is used in an effective manner allows for a reduction in its overall consumption, which in turn cuts down on the quantity of fuel that is required to power those turbines.

2.3. Offshore drilling rig based on renewable energy

Energy that originates from a system that fails to deplete over time is referred to as "renewable energy." They are natural, they can regenerate themselves, and their carbon impact is often very little or nonexistent. Wind energy, solar energy, bioenergy, and hydroelectricity, particularly ocean tidal energy, are all forms of clean energy. Tidal power is also a kind of hydroelectricity. alternative power for use in offshore applications because of their ability to supply a limitless quantity of renewable power. Throughout the

present day, significant initiatives have been launched to create a more sustainable energy industry by diverting attention from the use of carbon fuels to the practice of renewable energy resources. The goal of these endeavors is to decrease the pace at which fossil fuels are nowadays being utilized as well as the consequences that this has on the climate. The substitution of traditional fuels used to power oil and gas drilling platforms with clean power sources, including offshore wind, energy from the sun, as well as tidal power, is one of the primary focuses of a pilot project now underway. A number of offshore installations have indeed begun using green energy sources to create power sources in order to cut down on the amount of petroleum they need to purchase. For instance, the offshore energy station inside the southern part of the North Sea depicted in Fig. 1(a) is able to function because it generates its own electricity via the use of wind turbines and solar panels.

2.4. Future challenges

The future challenge is to generate maximum solar energy from the solar energy which is used in the rig for navigation and other purposes and most effectively used at night. It is common nowadays that nanotechnology somehow minimizes this challenge. It is detected that nanoparticles amplify the thermal conducting of the fluid.

2.4.1. How to overcome this challenge?

According to what the researchers found, putting nanoparticles in something is like putting millions of tiny reflectors inside a solar cell. As the light from the sun passes through the device, it strikes the nanoparticles, causing the light to scatter and possibly strike additional nanoparticles. This makes the light bounce around inside the device many times, which makes the photocurrent go up a lot.

2.4.2. Motive and mechanism of the present study present study

Present study is planned to investigate the outcome of novel tetra hybridity nanomolecules utilizing the Xue nanofluid model accompanied with heat transfer enhancing effects like nonlinear thermal radiation, thermal conductivity, and homogeneous/heterogeneous reactions on stretching sheet located below the photovoltaic cell sheet of PV panel located on the top of the rig. The solar PV plate is detected interior the glass sheet. When solar rays exist on the plate of the solar sheet the rays penetrated through PV sheet and fall on the sheet on which tetra hybrid nanofluid is flowing. The thermal conductivity of fluid amplifies. Catalytic reactions enhance the chemical reaction between nanoparticles and base fluid.

2.4.3. Advantages of using solar PV panels instead of diesel generators

- No risk of fire on the rig's stationery.
- Computational cost is low.
- Clean atmosphere and no noise pollution.
- Minimal maintenance is required.
- Green until the end of life.

2.4.4. Nanoparticles used in the present study

Copper is used a lot in the solar industry because it is cheap and can be found in many places. The amount of light absorbed in the DSSC's photo-anode layer is improved by the use of silver nanoparticles (AgNPs). Nanoparticles (NPs) are used in DSSCs not just to increase individual PCEs by boosting the cells' fluorescence intensity, but also to modify the cells' electron dynamics. Surface chilling employing Al_2O_3 increases solar cell performance, which in turn enhances the productivity of photovoltaic panels and decreases

Fig. 1(a). Solar Powered offshore platform.

greenhouse gas emissions. Increased carrier charge production and conductance were achieved in the TiO_2 nanoparticle/nanotube-based cells by increasing their exposure to sunlight (Fig. 1(b)).

3. Cost analysis of diesel generator vs solar panels in the case of Pakistan

3.1. Energy requirement

Offshore rigs require 1000–3000 hp. Diesel generators often provide energy. Based on activity, such engines consume 20–30 m^3 of fuel daily. Shown is a subsea rig. The hoisting but also liquid circulation devices use the greatest amount of energy on a rig, whereas the rotary, well control, and surveillance systems use less. Oil and gas setups are using energy to run pumps to retrieve crude oil, in order to extract oil, gas, as well as water from either the bit stream, drive compressors but also pump systems to move petroleum and natural gas via gathering pipes to treatment facilities, as well as power compressors but also pumps to produce hot water and electricity like on-site activities and living quarters, the production stream must be heated.

3.2. Need for solar panels instead of power fuels

The number of modules required in the case of solar panels to replace power fuel is given by

$$No\ of\ modules = \frac{kwh\ needed\ per\ day}{peak\ sun\ light\ hours\ per\ day \times power\ rating\ of\ PV\ cell/1000\ kw}$$

Peak hours of solar light in the area of Karachi tropic region ranges between 3 and 9 h average of 6 h moreover the power of PV cell used is 320 W. Then the energy used during living quarters is 9600 kwh/day. Then the requirement of modules are

$$No\ of\ modules = \frac{9600}{6 \times 320/1000}$$

Hence, considering no inefficiencies, at minimum 5000 solar panels will really be sufficient to generate sufficient energy for such dwellings.

The size of solar plates ranges between 1.6 m and 0.9 m giving an approximate area of 1.44 m^2 then space required for the case of 5000 modules are

$$Space\ required = 5000 \times 1.44 = 7200 m^2$$

Thus, if there are no losses, 7200 photovoltaic arrays should be enough to supply enough electricity for these kinds of dwellings.

3.3. Cost calculation

Due to different operations performed on the rig located near the exact cost Karachi coast on Indus G-Block (Kekra-1) in Pakistan. It is difficult to estimate the exact cost of solar installation on the rig. Let for the sake of comparison cost we choose laundry operation on the rig requires 12Kw power in an hour and this power is easily achieved from solar energy this power can be easily utilized because laundry operation can be performed in the daytime without harm to other operations. Cost for diesel power. It was thought that a Cummins Model 13.5MDKDN offshore diesel engine providing 13.5 kW was being utilized to operate a 12 kW laundry purpose under full usage. Following the company's recommendations, this engine consumes 4.5 L of fuel an hour when operating at maximum capacity [49]. Whether this rig is functional in tropical Karachi offshore.

Diesel price in Pakistan = US$1.070 per liter as of March 5, 2023.

Cost of diesel per day in Pakistan = 1.070 × 4.5 = 4.815× 24 h = US$ 115.56

Cost of diesel per year in Pakistan = US$ 115.56 × 365 days = US$ 42791.4

Cost of diesel for laundry for 20 years in Pakistan = US$42791.4 × 20 = US$855828

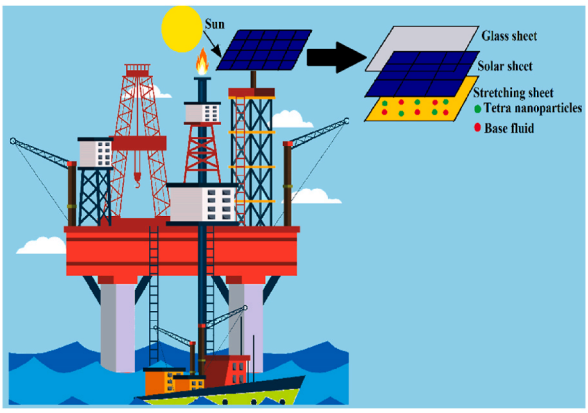

Fig. 1(b). Mechanism of the proposed model.

3.4. Cost of solar power

Power consumption of 12-kW equipment, in kilowatt-hours (kWh), is around 8640 every month. Experienced solar installer quotes in Pakistan could not be obtained in time for the research. The 81.18 kW maximum solar power plant may generate 8759 kWh every month being placed in a region receiving 5.04 kWh/m^2 bright sunshine hours across the United States, according to Solar-Estimate, a major solar power systems calculator. An estimated cost for the assembly was reported at around US$286130 [50]. The United States was chosen owing to the abundance of information about the subject of renewable power providers in that country's extensive web documentation. There are many tropical climate areas, and indeed, the nation is highly advanced because of its extensive petroleum sector. Oil platforms working in Pakistan are constructed in developed nations with advanced economies, much like the United States. It seems logical to use the United States as either a case study or benchmark for estimating solar energy costs since every solar energy installation will probably get bought there. The additional cost of 50% of the original solar panel installation must be added in terms of the replacement of damaged PV modules, batteries, and other occasional repairs over the period of 20 years. The total cost for the period of 20 years is US$ 429195.

3.5. Cost difference between solar panels and diesel generators

Calculated cost comparisons revealed that switching from diesel generators to solar power could save US$ 426633 (49%) over 20 years if the entire offshore Indus G-Block (Kekra-1) in Pakistan were to do so.

4. Geometry of the statement

A demonstration of the physical problem is described in Fig. 1(c). Solar rays directly coming from the sun falls on PV solar panel mounted on top of the rig. Thes Solar rays passed through the glass sheet and entered via the solar PV plate and fall on tetrahybrid nanofluid moving over an expandable sheet. three-dimensional materials that do not compress Flow of a cross-hybridity nanoliquid occurs when the fluid is subjected to the influences of a nonlinear phenomenon-based electromagnetic radiation, catalytic chemical processes, variable thermal conductivity, and an angled magnetic field. The total temperature of the fluid is increased along with the amount of heat that is created because of phenomena such as varying thermal conductance, thermal radiative fluxing, and tetra nanomolecules. To study the effect that tetrahybrid nanoparticles have when combined with ethylene glycol as the conventional liquid, the Xue tetra hybrid nanofluid model is being taken into consideration. Homogeneous/heterogeneous chemical reactions are considered for the investigation of reactants and products. In the present formulation, catalysis reactions are considered in order to enhance the impact of the chemical reaction between nanoparticles and base fluid. Furthermore, the assumption of isothermal cubic autocatalytic reaction is made here by the equation

$$\left.\begin{array}{c} \overline{E}+2\overline{F}\rightarrow 3\overline{F}, \textit{and its rate is given by} \\ \textit{rate}=\overline{G}_a\overline{G}_b. \end{array}\right\} \tag{1}$$

While the single and first-order isothermal cubic autocatalytic reaction is given

$$\left.\begin{array}{c} \overline{E}\rightarrow\overline{F}, \textit{and its rate is given by} \\ \textit{rate}=\overline{k}_s\overline{G}_a. \end{array}\right\} \tag{2}$$

Flow is considered over the place $z=0$ and it is confined in the region of $z>0$. Convective boundary conditions are incorporated to maintain a constant temperature. $u_w(x)$ is a component of the velocity of the fluid along $x-$ axis and $v_w(x)$ is along the $y-$ axis. C_∞, C_w, T_∞, and T_f are ambient concentration, nanoparticles concentration, ambient temperatures, and temperatures respectively [11].

$$\frac{\partial u}{\partial x}+\frac{\partial v}{\partial y}+\frac{\partial w}{\partial z}=0, \tag{3}$$

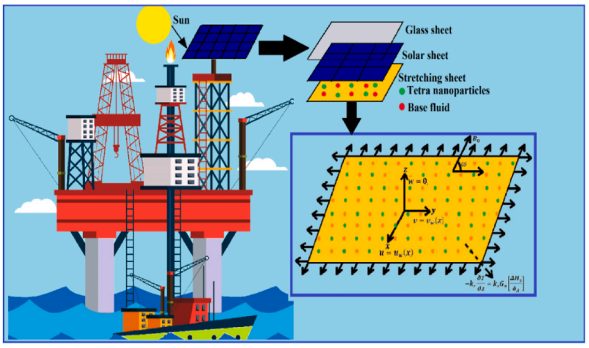

Fig. 1(c). Geometric depiction of flowing simulation.

$$\frac{\partial u}{\partial t}+u\frac{\partial u}{\partial x}+v\frac{\partial u}{\partial y}+w\frac{\partial u}{\partial z}=-\frac{1}{\rho_{tethnf}}\frac{\partial p}{\partial x}+\frac{\mu_{tethnf}}{\rho_{tethnf}}\frac{\partial}{\partial z}\left[\frac{\frac{\partial u}{\partial z}}{1+\left(\Gamma\frac{\partial u}{\partial z}\right)^{n}}\right]-\frac{\sigma_{tethnf}B_0^2\,sin^2(\omega)}{\rho_{tethnf}}u, \tag{4}$$

$$\frac{\partial v}{\partial t}+u\frac{\partial v}{\partial x}+v\frac{\partial v}{\partial y}+w\frac{\partial v}{\partial z}=-\frac{1}{\rho_{tethnf}}\frac{\partial p}{\partial y}+\frac{\mu_{tethnf}}{\rho_{tethnf}}\left[\frac{\frac{\partial v}{\partial z}}{1+\left(\Gamma\frac{\partial v}{\partial z}\right)^{n}}\right]-\frac{\sigma_{tethnf}B_0^2\,sin^2(\omega)}{\rho_{tethnf}}v, \tag{5}$$

$$\frac{\partial T}{\partial t}+u\frac{\partial T}{\partial x}+v\frac{\partial T}{\partial y}+w\frac{\partial T}{\partial z}=\frac{1}{(\rho c_p)_{tethnf}}\frac{\partial}{\partial z}\left\{k_{tethnf}(T)\frac{\partial T}{\partial z}\right\}-\frac{k_1G_aG_b^{\,2}}{(\rho c_p)_{tethnf}}\left[-\frac{\Delta H_h}{\delta_A}\right]-\frac{1}{(\rho c_p)_{tethnf}}\frac{\partial q_r}{\partial z}, \tag{6}$$

$$\frac{\partial G_a}{\partial t}+u\frac{\partial G_a}{\partial x}+v\frac{\partial G_a}{\partial y}+w\frac{\partial G_a}{\partial z}=D_A\frac{\partial^2 G_a}{\partial z^2}-k_1G_aG_b^{\,2}, \tag{7}$$

$$\frac{\partial G_b}{\partial t}+u\frac{\partial G_b}{\partial x}+v\frac{\partial G_b}{\partial y}+w\frac{\partial G_b}{\partial z}=D_A\frac{\partial^2 G_b}{\partial z^2}-k_1G_aG_b^{\,2}, \tag{8}$$

The boundary conditions are

$$\left.\begin{aligned} u=u_w(x),v=v_w(x),w=0,-k_r\frac{\partial T}{\partial z}=k_sG_a\left[\frac{\Delta H_s}{\delta_A}\right]\\ D_A\frac{\partial G_a}{\partial z}=k_sG_a,D_B\frac{\partial G_b}{\partial z}=-k_sG_a\text{ at }z=0,\end{aligned}\right\} \tag{9}$$

here,

$$u_w(x,t)=\frac{bx}{1-\beta t},v_w(x,t)=\frac{by}{1-\beta t}, \tag{10}$$

$$u\to 0,G_a\to G_\infty,G_b\to 0,v\to 0,T\to T_\infty\text{ as }z\to\infty. \tag{12}$$

Following are mathematical formulations that describe the thermophysical features of the expanded version of trihybridity nanofluid [27,28] to tetra hybridity nanofluid (tethnf).

$$\left.\begin{aligned}
&\mu_{tethnf}=\frac{\mu_f}{(1-\phi_1)^{2.5}(1-\phi_2)^{2.5}(1-\phi_3)^{2.5}(1-\phi_4)^{2.5}},\\
&\rho_{tethnf}=\left[(1-\phi_4)\left\{(1-\phi_3)(1-\phi_2)\left[(1-\phi_1)\rho_f+\rho_1\phi_1\right]+\rho_2\phi_2+\rho_3\phi_3\right\}+\rho_4\phi_4\right],\\
&(\rho C_p)_{tethnf}=(1-\phi_4)\left\{(1-\phi_3)(1-\phi_2)\left[(1-\phi_1)(\rho C_p)_f+(\rho C_p)_{s_1}\phi_1\right]+(\rho C_p)_{s_2}\phi_2+(\rho C_p)_{s_3}\phi_3\right\}+(\rho C_p)_{s_4}\phi_4,\\
&\frac{k_{tethnf}}{k_{thnf}}=\frac{1-\phi_4+2\phi_4\left(\frac{k_{s_4}}{k_{s_4}-k_{thnf}}\right)ln\frac{k_{s_4}+k_{thnf}}{2k_{thnf}}}{1-\phi_4+2\phi_4\left(\frac{k_{thnf}}{k_{s_4}-k_{thnf}}\right)ln\frac{k_{s_2}+k_{thnf}}{2k_{thnf}}},\frac{k_{thnf}}{k_{hnf}}=\frac{1-\phi_3+2\phi_3\left(\frac{k_{s_3}}{k_{s_3}-k_{hnf}}\right)ln\frac{k_{s_3}+k_{hnf}}{2k_{hnf}}}{1-\phi_3+2\phi_3\left(\frac{k_{hnf}}{k_{s_1}-k_{hnf}}\right)ln\frac{k_{s_1}+khn_f}{2k_{hnf}}},\\
&\frac{k_{hnf}}{k_{nf}}=\frac{1-\phi_2+2\phi_2\left(\frac{k_{s_2}}{k_{s_2}-k_{nf}}\right)ln\frac{k_{s_2}+k_{nf}}{2k_{nf}}}{1-\phi_2+2\phi_2\left(\frac{k_{bf}}{k_{s_2}-k_{nf}}\right)ln\frac{k_{s_2}+k_{nf}}{2k_{nf}}},\frac{k_{nf}}{k_f}=\frac{1-\phi_1+2\phi_1\left(\frac{k_{s_1}}{k_{s_1}-k_f}\right)ln\frac{k_{s_1}+k_f}{2k_f}}{1-\phi_1+2\phi_1\left(\frac{k_f}{k_{s_1}-k_f}\right)ln\frac{k_{s_1}+k_f}{2k_f}},\\
&\frac{\sigma_{tethnf}}{\sigma_{thnf}}=\frac{(1+2\phi_4)\sigma_4+(1-2\phi_4)\sigma_{tethnf}}{(1-\phi_4)\sigma_4+(1+\phi_4)\sigma_{tethnf}},\frac{\sigma t_{hnf}}{\sigma_{hnf}}=\frac{(1+2\phi_3)\sigma_3+(1-2\phi_3)\sigma_{hnf}}{(1-\phi_3)\sigma_3+(1+\phi_3)\sigma_{hnf}},\\
&\frac{\sigma_{hnf}}{\sigma_{nf}}=\frac{(1+2\phi_2)\sigma_2+(1-2\phi_2)\sigma_{nf}}{(1-\phi_2)\sigma_3+(1+\phi_2)\sigma_{nf}},\frac{\sigma_{nf}}{\sigma_f}=\frac{(1+2\phi_1)\sigma_1+(1-2\phi_1)\sigma_f}{(1-\phi_1)\sigma_1+(1+\phi_1)\sigma_f},
\end{aligned}\right\} \tag{13}$$

The symbols ϕ_1, ϕ_2, ϕ_3, ϕ_4, μ_{tethnf}, ρ_{tethnf}, k_{tethnf}, $(\rho C_p)_{tethnf}$, k_{thnf}, k_{nf}, k_f, $(\rho C_p)_f$ indicates the fractional size of nanomolecules (s_1, s_2, s_3, s_4), the dynamic viscosity of tetra nanomolecules, the density of ternary hybridity nanomolecules, the thermal conductance of tetra nanomolecules, the specific heat of tetra hybrid nanoparticles, the thermal conductance of ternary hybridity, dihybridity, and mono HNFs, and the specific heat of the liquid, correspondingly. Ethylene glycol ($C_2H_6O_2$) is considered as the base fluid whereas Ag, TiO_2, Cu, and Al_2O_3 with properties mentioned in Table 1

By implementing the appropriate conversions

$$\left.\begin{array}{c} \varphi(\eta)=\dfrac{G_b}{G_\infty},\theta(\eta)=\dfrac{T-T_\infty}{\Delta T},\vartheta(\eta)=\dfrac{G_a}{G_\infty},w=\sqrt{\dfrac{va}{1-\beta t}}(f(\eta)+g(\eta)) \\ u=\dfrac{ax}{1-\beta t}f^{'}(\eta),v=-\dfrac{ay}{1-\beta t}g^{'}(\eta),\eta=z\sqrt{\dfrac{a}{[1-\beta t]\nu}}, \end{array}\right) \tag{14}$$

After the utilization of the above-mentioned transformation, we got a subsequent scheme of ODEs.

$$[1-(n-1)(Wef'')^n]f'''+A_1A_2S[(f+g)f'']\left(1+(Wef'')^n\right)^2-A_1A_2\left(1+(Wef'')^n\right)^2\left[S\left(f'+\frac{\eta}{2}f'\right)+f'^2+A_3M^2\ sin^2(\omega)f'\right]=0, \tag{15}$$

$$\left[[1+(Weg'')^n]g'''+A_1A_2[(f+g)g'']\left(1+(Weg'')^n\right)^2-A_1A_2\left(1+(Weg'')^n\right)^2\left[S\left(g'+\frac{\eta}{2}g'\right)+g'2+A_3M^2\ sin^2(\omega)g'\right]=0,\right. \tag{16}$$

$$\frac{d}{d\eta}\left[(1+Rd(\theta_w-1)\theta)^3\theta'\right]+Pr[\varepsilon\theta]\theta''+Pr\ \varepsilon\theta'2-Pr\left[S\frac{\eta}{2}\theta'-R_H(1-\vartheta)^2\vartheta-(f+g)\theta'\right]=0, \tag{17}$$

$$\vartheta''+Sc\left[(f+g)\vartheta'-K\varphi^2\vartheta-S\frac{\eta}{2}\vartheta'\right]=0, \tag{18}$$

$$\varphi''+Sc\left[(f+g)\varphi-K\varphi^2\vartheta-S\frac{\eta}{2}\varphi'\right]=0. \tag{19}$$

Use ipdentity

$$\vartheta+\varphi=1\Rightarrow\vartheta=1-\varphi\ or\ \varphi=1-\vartheta \tag{20}$$

$$\vartheta''+Sc\left[(f+g)\vartheta'-K(1-\vartheta)^2\vartheta-S\frac{\eta}{2}\vartheta'\right]=0. \tag{21}$$

Having BCs $\vartheta'(0)=k_s\vartheta(0)$ and $\vartheta(\infty)=1$.
Overall boundary constraints of the modeled PDEs become as:

$$\left.\begin{array}{c} f(0)=0,g(0)=0,w=0, \\ f'(0)=1,g'(0)=\lambda, \\ f'(\infty)=0,g'(\infty)=0 \\ \theta'(0)=-K_r(1-\vartheta(0)),\vartheta'(0)=k_s\vartheta(0), \\ \theta(\infty)=0,\vartheta(\infty)=1 \end{array}\right\} \tag{22}$$

The parameters used in the above equations 9–12 are given as:

$$We=\Gamma ax\left(\sqrt{\frac{a}{\nu(1-\beta t)}}\right),M=\frac{\sigma B_0^2}{\rho_f a}(1-\beta t),R_H=K_1\frac{\Delta H_h}{\delta_A}\frac{1}{(\rho c)_f}\frac{{G_\infty}^2}{a\Delta T}(1-\beta t),$$

$$K=\frac{k_1{G_\infty}^2}{a}(1-\beta t),Sc=\frac{\nu}{D_A},\lambda=\frac{b}{a},\theta_w=\frac{T_w}{T_\infty},S=\frac{\beta}{a},Rd=\frac{16\sigma^*T_\infty^3}{3k^*k},$$

$$Pr=\frac{\nu}{\alpha},\varepsilon=\frac{D_B}{D_A},$$

The frictional force factor and shearing stresses are indicated and described as

$$\left.\begin{array}{c} C_{fx}=\left(\dfrac{2\tau_{xz}}{\rho u^2}\right)\Rightarrow(Re_x)^{-0.5}C_{fx}=\dfrac{1}{A_1}\left(\dfrac{2f''}{1+(Wef'')^n}\right), \\ C_{fy}=\left(\dfrac{2\tau_{yz}}{\rho u^2}\right)\Rightarrow(Re_x)^{-0.5}C_{fy}=\dfrac{1}{A_1}\left(\dfrac{2g''}{1+(Weg'')^n}\right), \\ Nu_x=\left(\dfrac{xq_w}{k\left(T_f-T\right)}\right)\Rightarrow(Re_x)^{-0.5}Nu_x=-A_4\left(1+(1+Rd(\theta_w-1)\theta)^3\right)\theta'(0). \end{array}\right\} \tag{23}$$

Table 1
Thermophysical characteristics.

Property	EG	Ag	TiO_2	Cu	Al_2O_3
ρ	1114	10500	4250	8933	3970
C_p	2415	235	690	385	765
k	0.252	429	8.953	400	40
σ	4.3×10^{-5}	6.3×10^{7}	2.4×10^{6}	6×10^{7}	3.5×10^{7}

whereas A_1, A_2, A_3, A_4, A_5 are given by

$$\left.\begin{aligned} A_1 &= \frac{1}{(1-\phi_1)^{2.5}(1-\phi_2)^{2.5}(1-\phi_3)^{2.5}(1-\phi_4)^{2.5}}, \\ A_2 &= (1-\phi_4)\left\{(1-\phi_3)(1-\phi_2)\left[(1-\phi_1)+\phi_1\frac{\rho_1}{\rho_f}\right]+\phi_2\frac{\rho_2}{\rho_f}+\phi_3\frac{\rho_3}{\rho_f}\right\}+\phi_4\frac{\rho_4}{\rho_f}, \\ A_3 &= \frac{\sigma_{tethnf}}{\sigma_f}, \\ A_5 &= (1-\phi_4)\left\{(1-\phi_3)(1-\phi_2)\left\{(1-\phi_1)+\frac{(\rho C_p)_{s_1}}{(\rho C_p)_f}\phi_1\right\}+\frac{(\rho C_p)_{s_2}}{(\rho C_p)_f}\phi_2+\frac{(\rho C_p)_{s_3}}{(\rho C_p)_f}\phi_3\right\}+ \\ &\quad \frac{(\rho C_p)_{s_4}}{(\rho C_p)_f}\phi_4, \\ A_4 &= \frac{k_{tethnf}}{k_f}. \end{aligned}\right\} \tag{24}$$

5. Numerical procedure

To resolve formulas (9-10), which, when combined with endpoints restrictions (11), constitute the modeled issue, the Cash and Carp approach (11) is utilized. Because Cash and Carp's impacts seem to have a rounded error with order 5, they provide more favorable results than even a variety of those other methods (see Table 1). The interaction of formulas (9) via (10) is complicated, and analytical analyzing them is a task that takes a significant amount of time owing to the difficulty of the issue. The ultimate goal would be to carry out numerical analysis on the system of formulas while taking into account BCs (11). We have the ability to resolve formulas by applying our shooting abilities in combination with the RKF strategy. There are a number of different numerical algorithms that have been used in the past in order to answer these types of formulas. The complete procedure is commonly referred to as the "Cash and Carp" approach (Fig. 1(d)), which is a literal translation of the term. After the formulas have been converted into BVP problems by assigning symbols to the miss beginning circumstances, the shooting methodology, together with the RKF method, may be used effectively in BVP.

The 1st-order ordinary differential equations that have been derived from partial differential equations include

$$f = y_1, g = y_4, \theta = y_7, \vartheta = y_9, \tag{25}$$

to get

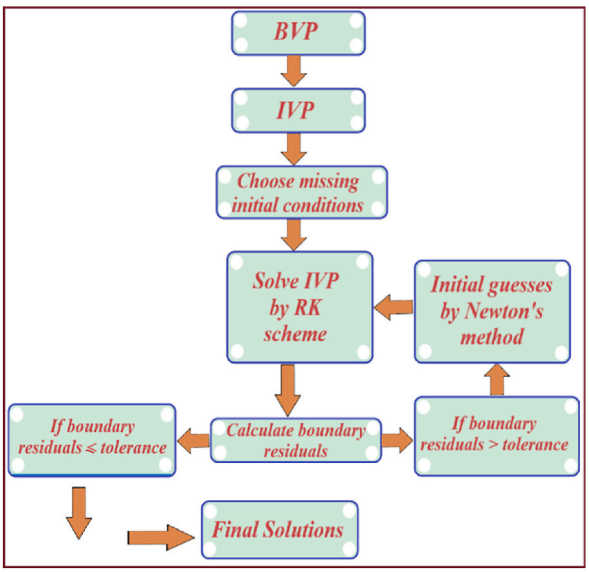

Fig. 1(d). Cash and carp process flow chart.

$$\left.\begin{aligned} f' &= y_2, f'' = y_3, \\ f''' = y_3' &= \frac{A_1A_2[1+(Wey_3)^n]^2\left[\left(y_2+\frac{\eta}{2}y_2\right)+A_3M^2\ sin^2(\omega)y_2+{y_2}^2-S(y_1+y_4)y_3\right]}{(1+(1-n)(Wey_3)^n)} \\ g &= y_4, g' = y_5, g'' = y_6, \\ f''' = y_3' &= \frac{A_1A_2[1+(Wey_3)^n]^2\left[\left(y_2+\frac{\eta}{2}y_2\right)+A_3M^2\ sin^2(\omega)y_2+{y_2}^2-S(y_1+y_4)y_3\right]}{(1+(1-n)(Wey_3)^n)}, \\ \theta &= y_7, \theta' = y_8, \\ \theta'' = y_8' &= \frac{-\frac{A_5}{A_4}\Pr\left(S\frac{\eta}{2}y_8-R_H(1-y_9)^2y_9-(y_1+y_4)y_8\right)-Pr\ \varepsilon{y_8}^2-3Rd(\theta_w-1)(1+(\theta_w-1)y_7)^2}{\left((1+\varepsilon y_4)+Rd(1+(\theta_w-1)y_7)^3\right)}, \\ \vartheta &= y_9, \vartheta' = y_{10}, \\ \vartheta'' = y_{10}' &= Sc\left(S\frac{\eta}{2}y_{10}+K(1-y_9)^2y_9-(y_1+y_4)y_{10}\right), \end{aligned}\right\} \tag{26}$$

BCs (6) are now

$$\left.\begin{aligned} &\eta = 0 : y_1(\eta) = 0, y_2(\eta) = \lambda, y_4(\eta) = 0, y_5(\eta) = \lambda, y_8\ (\eta) = -K_r(1-y_9), \\ &y_{10}\ (\eta) = Ksy_9, \eta\to\infty : y_2\ (\eta)\to 0, y_5\ (\eta)\to 0, y_7\ (\eta)\to 0, y_9\ (\eta)\to 1 \end{aligned}\right\} \tag{27}$$

In order to determine how to resolve the ODEs shown previously, the RKF of the fourth and fifth orders is employed.

$$\left.\begin{aligned} &\mathbf{K_1} = h\mathbf{F}(\eta, \mathbf{Z}), \\ &\mathbf{K_i} = h\mathbf{F}\left(\eta + A_i, \mathbf{Z} + \sum_{j=1}^{i-1} B_{ij}\mathbf{K_j}\right), i = 2, 3, ..., 6, \\ &\mathbf{Z_5}(\eta + h) = \mathbf{Z}(\eta) + \sum_{i=1}^{6} C_i\mathbf{K_i}, \\ &\mathbf{Z_4}(\eta + h) = \mathbf{Z}(\eta) + \sum_{i=1}^{6} D_i\mathbf{K_i}, \end{aligned}\right\} \tag{28}$$

a situation in which the equations of the fourth in addition to the fifth orders are signified by the indices 4 but also 5, accordingly. On the other hand, $\mathbf{K_1}$, $\mathbf{K_i}$, $\mathbf{F}$ and $\mathbf{Z}$ may nearly always be categorized as

$$\mathbf{K_1} = \begin{bmatrix} K_{11} \\ K_{12} \\ K_{13} \\ K_{14} \\ K_{15} \\ K_{16} \\ K_{17} \\ K_{18} \\ K_{19} \\ K_{110} \end{bmatrix}, \mathbf{K_i} = \begin{bmatrix} K_{i1} \\ K_{i2} \\ K_{i3} \\ K_{i4} \\ K_{i5} \\ K_{i6} \\ K_{i7} \\ K_{i8} \\ K_{i9} \\ K_{i10} \end{bmatrix}, \mathbf{F} = \begin{bmatrix} f_{11} \\ f_{12} \\ f_{13} \\ f_{14} \\ f_{15} \\ f_{16} \\ f_{17} \\ f_{18} \\ f_{19} \\ f_{110} \end{bmatrix}, \mathbf{Z} = \begin{bmatrix} z_{11} \\ z_{12} \\ z_{13} \\ z_{14} \\ z_{15} \\ z_{16} \\ z_{17} \\ z_{18} \\ z_{19} \\ z_{110} \end{bmatrix}, \tag{29}$$

in where i may take the values $i = 2, 3, ...6$. The factors used in the RKF equation can be found listed below in Table 2.

The procedure of finding a solution to the issue calls for serious examination of the route length h that is being applied. In relation to the matter at hand, the value 0.1 has been assigned to the attribute that is measured by h. It is possible to do a numerical investigation of equations 19–21 through employing the approach for this kind of fifth order. The method for the fourth order is only applicable for

Table 2
The mathematical illustrations of the indicators that Cash and Carp have made available.

i	A_i			B_{ij}			C_i	D_i
1	–	–	–	–	–	–	37/378	2825/27648
2	1/5	1/5	–	–	–	–	0	0
3	3/10	3/40	9/40	–	–	–	250/621	18 575/48384
4	3/5	3/10	9/40	6/5	–	–	125/594	13 525/55296
5	1	11/54	5/2	70/27	35/27	–	0	277/14336
6	7/8	1631/55296	175/512	575/13824	44275/110592	253/4096	512/1771	1/4

the truncation error reasons that are detailed later down in this passage.

$$E(h) = Z_5(\eta + h) - Z_4(\eta + h) = \sum_i (C_i - D_i)K_i \tag{30}$$

The difference that occurs between numbers that have been numerically computed and boundary values is referred to as the "residual" in this context. When the variance between the residuals at the border is less than the tolerance level of 10^{-8} to improve the original constraints that were not there, the final outcome has been obtained. This occurs whenever the initial restrictions did not exist. Newton's iterative approach of solving problems is put to use here. The following criteria will be used to ascertain whether or not the process of iteration has reached its conclusion:

$$\max\{|z_2(\eta_{max}) - 0|, |z_5(\eta_{max}) - 0|, |z_7(\eta_{max}) - 0|, |z_9(\eta_{max}) - 1|\} < 10^{-8} \tag{31}$$

The RKF approach makes use of a variety of coefficients, and Table 2 offers an example of several of these factors. The corresponding values are shown in the following table.

In an effort to demonstrate that the mathematical method is reliable, we compared our results to those that had been acquired in the past by Reddy et al. [22] with missing *Rd*. Not only did we find that there was a significant amount of concordance between the two groups of data, but we also found that there was a perfect match between the two groups of data.

6. Results and discussion

6.1. Sundry parameters effect on the velocity field

Current study did a numerical investigation regarding cubic autocatalysis and inclined magnetized velocity slip Carreau nanofluid with an artificial neural network (NN) and bvp4c method. Temperature-dependent thermal conductivity and homogeneous-heterogeneous chemical reactions are utilized in concentration and temperature profiles. Several parameters affiliated with all distribution profiles are shown by graphs and statistical tables.

The number that Weissenberg came up with is associated with unwinding. The amount of time that a liquid needs to relax. The decrease in viscosity that occurs because of an increase in *We* also causes a reduction in the rapidity field. As can be seen in Fig. 2(a), as the shearing viscosity of the liquid decreases, this results in an increase in the average speed of the liquid. The Weissenberg number, which is suited to characterize flows with a consistent stretch history, such as simple shear, specifies the degree of anisotropy or direction caused by the deformation. Physically dimensionless number (*We*) contrasts the viscous and elastic forces. It is well established that viscous forces topple elastic forces under an expansion in (*We*) which provides conflict to the liquid flowing and diminishes the velocity field $f'(\eta)$. It is quite evident that tetra hybrid nanoparticles (TETHNF) nanoparticles suspension in the base amplifies fluid concentration and overall density of the fluid which reduces the fluid speed and $f'(\eta)$. The purpose of Fig. 2(b) is to analyze the performance of n in comparison to $f'(\eta)$. The viscosity of the liquid is represented by the symbol *n*, which provides this information. Viscosity increases when *n* is more than one, is constant when *n* is equal to one (Newtonian) and decreases when *n* is one or less. The inertia of the liquid is overcome by the viscosity, which results in an increase in *n* and a decrease in $f'(\eta)$. Products used in everyday life such as ketchup, paint, blood, spaghetti, and other polymers are examples of substances whose viscosity may alter over time. Because of an incremental change in the fractional size of nanomolecules (TETHNF), which additionally reduces $f'(\eta)$, physically viscous forces predominate over inertial forces. This occurs because of an incremental change in the fractional size of nanomolecules. The influence

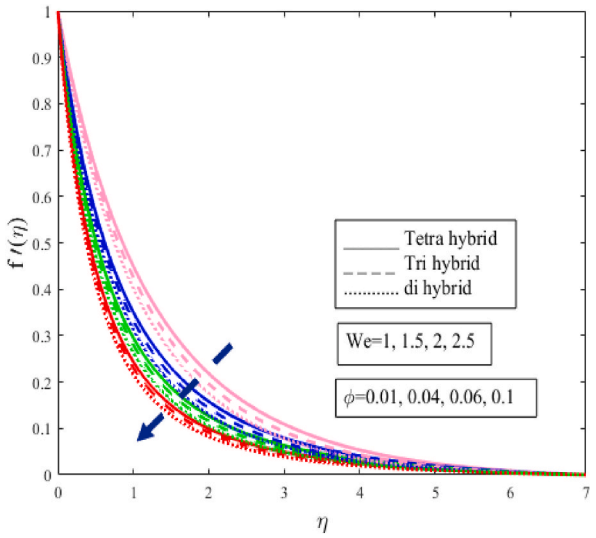

Fig. 2(a). Impact of Weissenberg number *We* on the velocity field $f'(\eta)$.

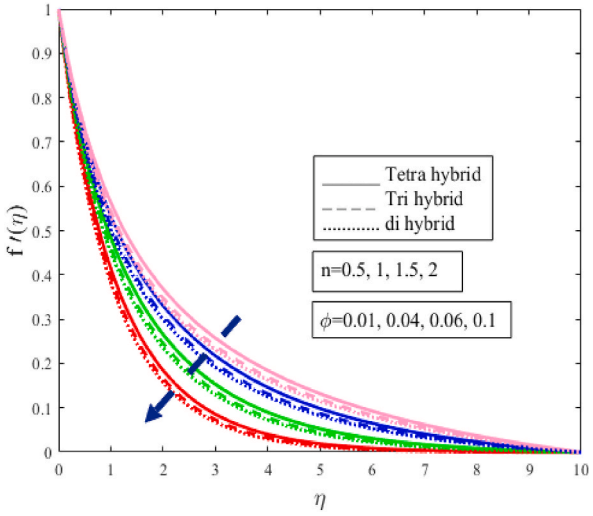

Fig. 2(b). Influence of viscosity index n on the velocity field $f'(\eta)$.

that the magnetic parameter M has on the frequency $f'(\eta)$ is reflected in the design of Fig. 2(c). It has been noticed that an electrically conducting liquid, while traveling through an electric field, produces a force known as the Lorentz force. This force is essentially resistive and resists fluid when it is exposed to an expanding sheet. Additionally, this force causes a reduction in the rapidity outline $f'(\eta)$ There is a movement of liquid in the direction of the vertical wall. The fluid velocity also diminishes by positive variation in $\omega = 0$ to $\frac{\pi}{2}$. It is quite evident that magnification in ω strengthens viscous-type forces which amplify the viscosity phenomenon and lessens $f'(\eta)$ displayed in Fig. 2(d). Lorentz force amplifies under enrichment in an inclined magnetic field ω which lessens $f'(\eta)$.

6.2. *Effect of sundry parameters on temperature field*

Fig. 3(a) draws attention to the impact that the radiation parameter Rd has on $\theta(\eta)$. Nonlinear thermal radiation is utilized in the case where the high-temperature difference is required and in the present model these rays are actually solar rays coming from the sun which are absorbed by the sheet located inside in PV sheet of a solar panel located on the top of the offshore oil rig. Physically electromagnetic radiation that passes through electromagnetic waves is known as thermal radiation. The movement of electrons and other components within a hot substance produces these forms of radiation. Due to the acceleration of the charge and the resulting dipole oscillation, electromagnetic radiation is produced. By increasing Rd, molecules have a greater chance of colliding with one another and sharing their kinetic energy, which in turn enhances the temperature outline. Thermal radiation is used in circumstances that demand a substantial temperature differential, and it has a broad variety of uses in industry, including nuclear reactors and burn reactors, amongst many others. Producing polymers, treating water, and other processes along the same lines are included. When Rd is increased, the degree of unpredictability in the collisions that take place between molecules also increases. The intensification of Rd

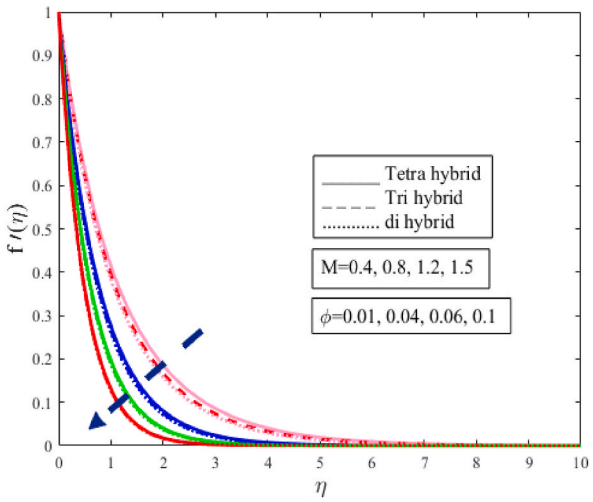

Fig. 2(c). Impact of magnetic parameter M on the velocity field $f'(\eta)$.

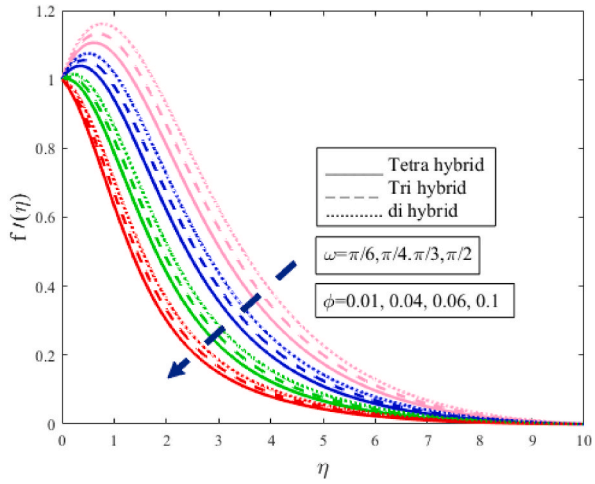

Fig. 2(d). Impact of inclined angle ω on the velocity field $f'(\eta)$.

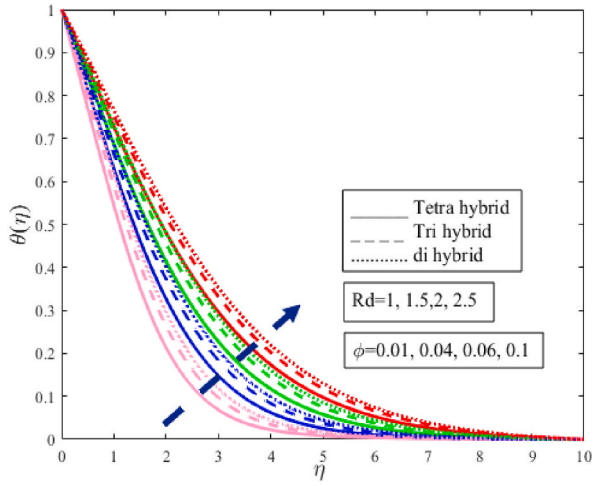

Fig. 3(a). Impact of inclined angle *Rd* on temperature field $\theta(\eta)$.

phenomenon that is brought about by the implantation of tetra nanocomposites into the base liquid leads to an increase in both $\theta(\eta)$ and the breadth of a temperature boundary layer. This is because the thickness of the temperature boundary layer increases. In the case of TETHNF, the radiation impact is amplified more so than when it is seen with THNF and HNF. The effect that the thermal conductance has on $\theta(\eta)$ is seen in Fig. 3(b). The capacity of a substance to transfer heat is referred to as its thermal conductivity. It has been shown beyond a reasonable doubt that the collision of fluid atoms results in an increase in the thermal conductivity of liquids. Physically thermal conductivity is a property that describes how well a material can conduct heat. It quantifies the rate at which heat energy is transferred through a material due to a temperature difference. The higher the thermal conductivity of a material, the better it is at conducting heat. Materials with high thermal conductivity, such as metals like copper and aluminum, are good conductors of heat. It's important to note that thermal conductivity can vary significantly depending on the material and its physical properties, such as density, composition, and temperature. The molecules in the fluid are able to transfer more of their kinetic energy to one another. As can be seen in the image, it is a fact that the TBL layer thickness increases greater for TETHNF as opposed to THNF. This fact has been well proven. The stretched sheet increases the dispersion of heat across the structure by amplifying, which in turn transmits additional heat throughout the system. Fig. 3(c) draws attention to the impact that the temperature ratio variable θ_w has on the value of $\theta(\eta)$.

Physically, when solar rays originating from the sun scatter on a stretched sheet, a chemical event known as a catalytic reaction begins to take place. This causes molecules to clash more randomly, which magnifies temperature conductance, and temperature conductance enhances even more in the existence of TETHNF. It should come as no surprise that the liquid is able to take in a greater quantity of heat as a direct consequence of the increase in θ_w, which in turn magnifies the thermal boundary thickness and temperature field $\theta(\eta)$. In fluid mechanics, the temperature ratio parameter can be important in analyzing compressible flow phenomena, such as in supersonic aerodynamics. The temperature ratio across a shock wave or an expansion fan can significantly affect the flow properties and behavior. In some applications, the temperature ratio parameter can be used to characterize the performance or efficiency of a

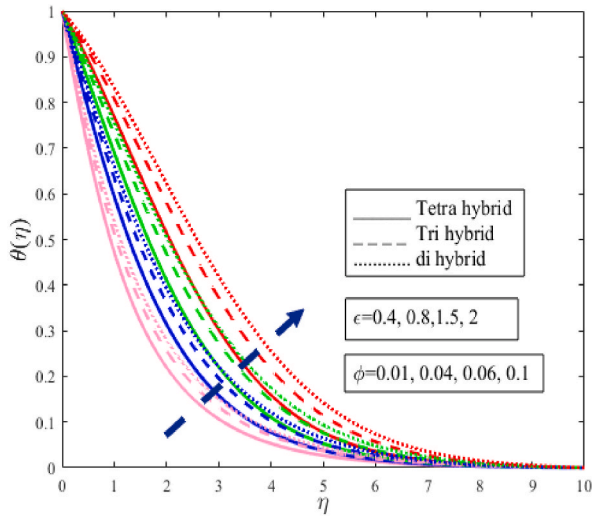

Fig. 3(b). Impact of thermal conductivity ε on temperature field $\theta(\eta)$.

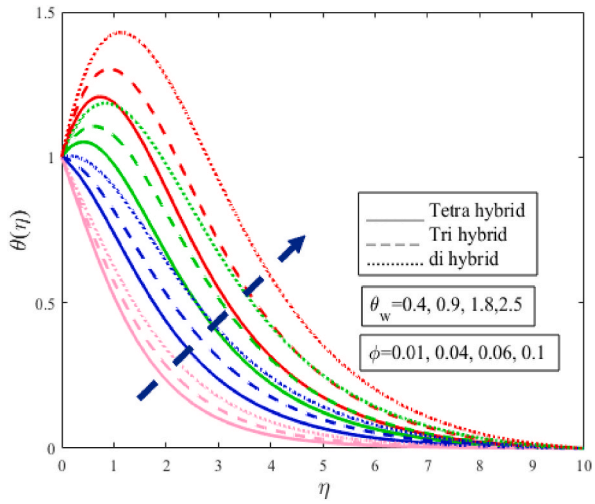

Fig. 3(c). Impact of temperature ratio parameter θ_w on temperature field $\theta(\eta)$.

system, particularly in thermodynamic cycles or heat transfer processes. Symbol θ_w represents wall temperature to ambient temperature. The temperature ratio parameter is a key factor of the nonlinear-based thermal radiation phenomenon. The temperature of the fluid rises as it moves upwards away from the stretching surface, which speeds up the rate at which heat is transferred inside the fluid. It is observed that heat transfer amplifies more in the case of TETHNF in contrast to THNF and simple HNF. A positive variation in *Pr* depreciates $\theta(\eta)$. Heat diffuses more quickly in the case of magnification in *Pr* which reduces heat transfer, as well as temperature phenomena, inside the liquid. The Prandtl number helps determine the dominant mode of heat transfer in a fluid. A low Prandtl number indicates that momentum diffusivity is dominant, meaning that the fluid tends to be more effective at transferring momentum than heat. Conversely, a high Prandtl number indicates that thermal diffusivity is dominant, implying that the fluid is more effective at transferring heat than momentum. Different fluids have different Prandtl numbers. For example, air and most gases have a Prandtl number close to 0.7, while water has a Prandtl number around 7. Prandtl number of ethylene glycol is 39. Physically these values influence the behavior of fluid flow and heat transfer in various applications, such as in the design of heat exchangers, boundary layer flows, and convection processes. Thermal boundary thickness diminishes in the case of *Pr* as shown in Fig. 3(d). Fig. 3(e) reflects the impact of concentration distribution R_H on $\theta(\eta)$. It is observed that the concentration distribution effect amplifies under magnification in a catalytic chemical reaction. A proper chemical reaction between TETHNF and fluid amplifies KE of the molecules and molecules of the fluid collide more randomly in the occurrence of TETHF and catalytic chemical reaction which amplifies temperature field $\theta(\eta)$. It is observed that heat transfers more in the case of TETHNF in contrast to THNF and HNF. More heat is absorbed by the solar panel located on an offshore oil rig by amplifying TETHNF, *Rd*, ε and R_H effects.

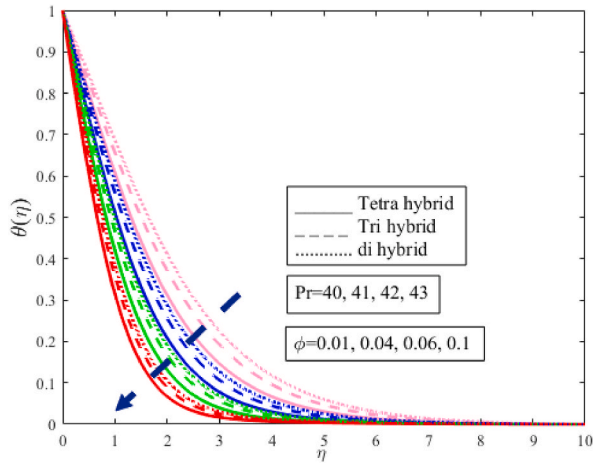

Fig. 3(d). Impact of Prandtl number *Pr* on temperature field $\theta(\eta)$.

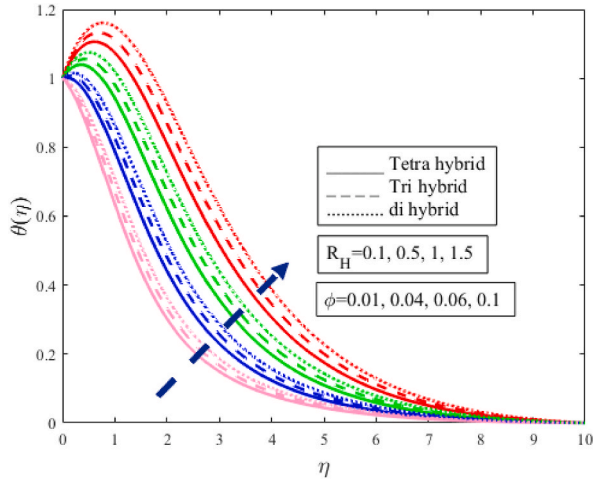

Fig. 3(e). Impact of R_H on temperature field $\theta(\eta)$.

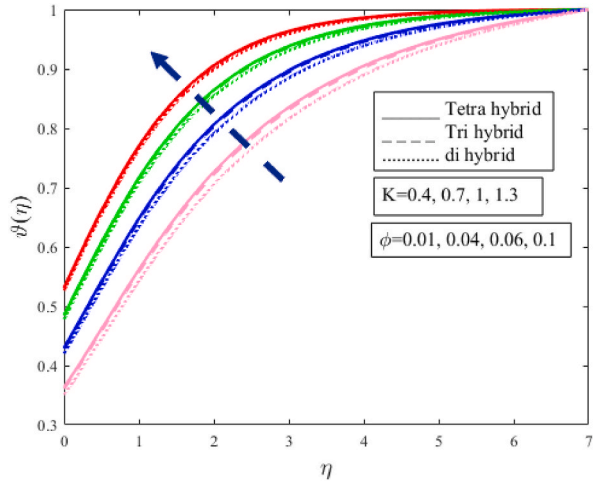

Fig. 4(a). Impact of homogeneous reaction *K* on concentration field $\vartheta(\eta)$.

6.3. Sundry parameters influence on concentration field

The effect that K has on the concentricity gradients is seen in Fig. 4(a). The concentricity gradients become more pronounced as K becomes higher in value. As the intensity of the homogeneous chemical reaction increases, a greater number of species are consumed in bulk, which leads to a decrease in the concentricity gradients represented by the symbol $\vartheta(\eta)$. In a homogeneous reaction where the concentration of a reactant decreases over time, the concentration profile typically exhibits an exponential decay pattern. The rate at which the concentration decreases depends on the reaction order and the specific rate constant associated with the reaction. Physically concentration profiles assume ideal conditions for a well-mixed homogeneous system. In reality, factors such as reaction mechanisms, reactant diffusion, and reactor design can affect the concentration profile and lead to deviations from these idealized patterns. Fig. 4(b) displayed the impact of Ks on $\vartheta(\eta)$. Diffusivity and concentricity are completely related with each other. Diffusivity is a property that quantifies how easily molecules or particles can move through a medium, while concentration refers to the amount of a substance per unit volume. Fick's Law of Diffusion describes the relationship between diffusivity, concentration, and the rate of mass transport. Physically higher diffusivity allows for faster diffusion, resulting in a higher mass flux for a given concentration gradient, while a lower diffusivity leads to slower diffusion and lower mass flux. In the event of a homogeneity reaction, both the liquid and the catalyst are present in an identical phase. This is one of the primary reasons for an increase in the concentration field and is also one of the most significant variables. Additionally, the flow diffusivity will change because of an increase in the value of the homogeneous reaction, which will result in a decrease in $\vartheta(\eta)$. Because an increase in the rate of change of the heterogeneous reaction's velocity signifies an increase in the number of chemical species participating in the chemical reaction on the chemical front, which, in turn, results in an increase in the concentricity of the chemical species. When Sc increases, there is a corresponding increase in the viscous diffusion that occurs in the scenario of fixed molecular diffusion. The Schmidt number has a close connection to the phenomena of diffusion and fills the same function in the equation for the concentration of a substance as the Prandtl number does in the equation for the energy it contains. There is a connection between the Schmidt number and the molecule diffusivity. It is abundantly obvious that a little modification in the molecular diffusivity results in an increase in the concentration of the fluid, which in turn leads to an amplification of the concentration issue. The Schmidt number is primarily used to determine the thickness of concentration boundary layers in a fluid flow. In general, a smaller Schmidt number indicates a higher diffusivity relative to viscosity, resulting in thinner concentration boundary layers. Conversely, a larger Schmidt number indicates a lower diffusivity relative to viscosity, leading to thicker concentration boundary layers. As can be seen in Fig. 4(c), when there is a rise in Sc, there is also a boost in $\vartheta(\eta)$, which causes the concentration of the fluid rising. It has been shown that momentum diffusivity increases when there is an augmentation in the fractional size of TETHF. This consequence also increases K but decreases Sc and Ks, and this impact is more pronounced when it occurs in the context of TETHNF in comparison to THNF and HNF.

6.4. Graphical representation of sundry parameters on physical quantities like drag friction coefficient and Nusselt number

Fig. 5(a) revealed the performance of n on the surface drag coefficient. The viscosity increases in terms of n moreover decreases the fluid velocity. The surface drag friction of the surface over which the fluid is moving amplifies owing to the decrement in n which amplifies the skin friction phenomenon. Generally the viscosity of a fluid increases, it leads to higher internal friction within the fluid. As a result, the fluid molecules exhibit greater resistance to flow, causing an increase in drag force. This means that a more viscous fluid will create more resistance and require more force to overcome compared to a less viscous fluid. However, if the viscosity becomes too high, it can increase the drag and result in decreased efficiency. The barrier to the flowing of the fluid is provided, physically speaking, by surface friction. When there is a positive change in the value of n, the viscosity of the fluid increases, which in turn reduces the fluid's velocity and makes the phenomena of surface drag more pronounced. In contrast to the effects of THNF and HNF, the presence of TETHNF causes the liquid to assume an additional concentrated state. The effect that the magnetic variable M has on the drag coefficient is seen in Fig. 5(b). The velocity of the liquid's flowing relative to a speed of the medium is what we refer to as surface drag. It has been observed that fluid speed reduces because of the multiplication in M, which lessens the effect of the surface drag phenomena. Drag friction, also known as fluid drag or air resistance, is primarily influenced by the interaction between a solid object and the surrounding fluid (such as air or water). However, in certain cases, a magnetic field can indirectly affect drag through the manipulation of the fluid or the object itself. By applying a magnetic field to the boundary layer, the electric currents induced can potentially influence the flow and reduce drag. It's important to note that the effectiveness of using magnetic fields to decrease drag friction depends on several factors, including the specific application, the strength and orientation of the magnetic field, and the properties of the fluid involved. The existence of a Lorentz force causes a fluid to become physically more viscous, and viscous forces dominate inertial forces, resulting in a decrease in fluid velocity and an increase in the impact of drag and friction. Fig. 5(c) draws attention to the impact that the Weissenberg number has on the surface friction caused by drag. The amount of time a fluid needs to relax before it can regain its former shape is linked to what is known as the Weissenberg number. In that period of time, the viscosity of the fluid will increase, making it difficult for the fluid to travel freely over the expanding sheet. The fluid's velocity will decrease as the magnification factor We increases. Relaxation time of the fluid amplifies in the case of magnification in tetra hybrid nanoparticles TETHNF which lessens the fluid speed. Drag friction is the friction caused by the fluid against the surface. It is well knowledge that an increase in We results in a decrease in velocity, which, on the other hand, results in an increase in the amount of drag and friction, as illustrated in Fig. 5(c). The Prandtl number Pr, remains the same even when the temperature changes, even though the temperature decreases within the fluid. Because there is a lower temperature within the liquid, heat can diffuse more rapidly under magnification in Pr, which finally leads to a lower Nusselt number for the transmission of heat, as illustrated in Fig. 5(d). Radiation parameter Rd is one of the crucial variables that need to be taken into consideration in order to magnify heat transmission. This parameter has enormous applications in thermal improvement, which are then used in combustion reactors, paper manufacture, polymer synthesis, and other

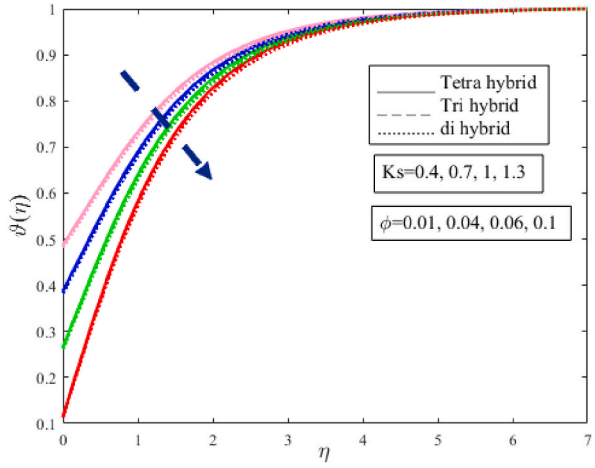

Fig. 4(b). Impact of heterogeneous reaction *Ks* on concentration field $\vartheta(\eta)$.

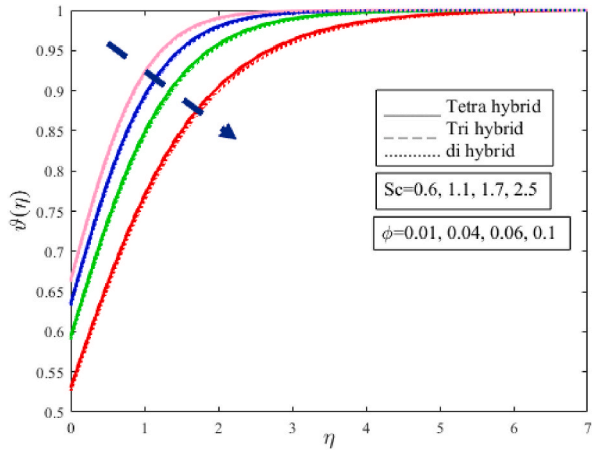

Fig. 4(c). Impact of Schmidt number *Sc* on concentration field $\vartheta(\eta)$.

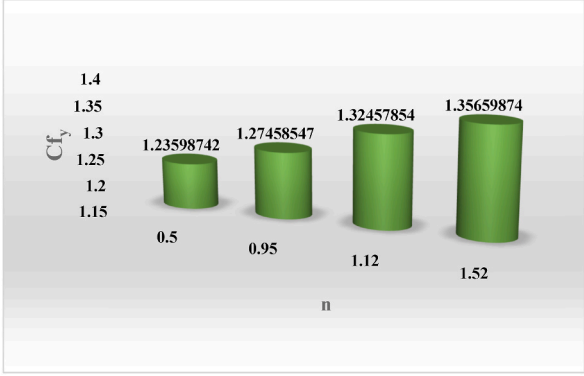

Fig. 5(a). Influence of *n* on skin friction.

processes. When thermal radiation is absorbed by an object, its energy is converted into heat, thereby increasing the object's temperature. The rate of heat transfer through thermal radiation depends on several factors, including the temperature difference between the objects, the emissivity of the surfaces involved, and the surface area of the objects. Thermal conductivity amplifies in the case of an incremental change in *Rd* which amplifies fluid temperature and the inclusion of nanoparticles in the base fluid amplifies *Rd*

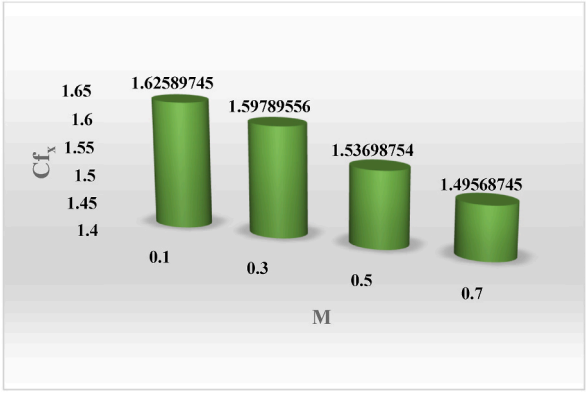

Fig. 5(b). Influence of *M* on skin friction.

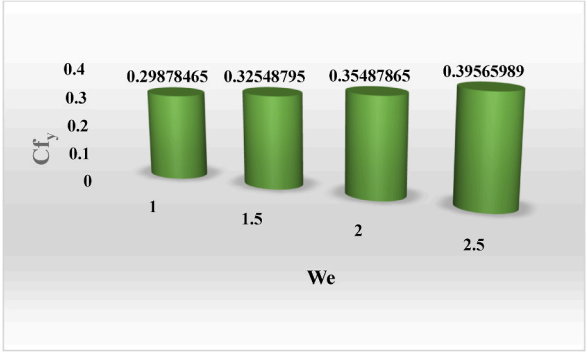

Fig. 5(c). Impact of *We* on the drag friction coefficient.

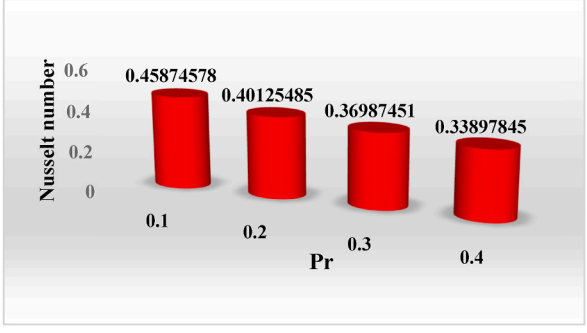

Fig. 5(d). Impact of *Pr* on Nusselt number.

phenomenon and amplifies the Nusselt number as shown in Fig. 5(e). Thermal radiation actually nonlinear thermal radiation is the key parameter to enhance heat trnasport rate in the case of solar PV panels located on the top of the offshore oil rig. The effect of *Rd* amplifies more and PV panel stores more energy in the presence of TETHNF. The parameters like thermal radiation, temperature ratio parameter, thermal conductivity, and tetrahybrid nanoparticles TETHF amplify the temperature and heat transfer rate of the fluid and transports more heat which is absorbed by the PV sheet and transfers more heat in the rig for drilling and navigational purposes.

6.5. *Streamlines behavior of sundry parameters on drag frictions and Nusselt numbers*

Fig. 6(a) illustrates a contour map that compares the velocity distribution to the porosity variable *n*. Increasing the accuracy of the estimates of *n* results in a decrease in the overall velocity. The contour justifications of rapidity versus *We* were shown in Fig. 6(b). It has been noticed that increasing *We* increases liquid speed and increases liquid speed causes a reduction in the viscosity of the liquid. In the form of a contour graph, Fig. 6(c) demonstrated the effect that *Rd* had on the temperature profile. Increasing *Rd* results in a rise in the temperature of the liquid. Increasing *Rd* causes an increase in temperature because it causes the fluid to absorb more heat. Fig. 6(d)

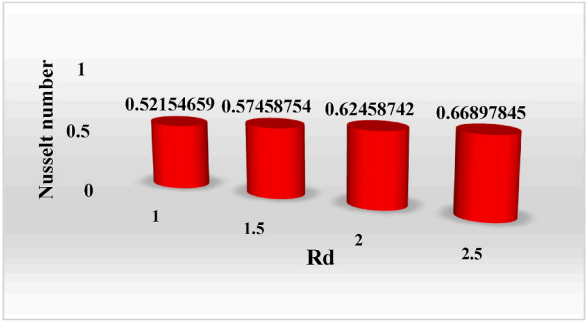

Fig. 5(e). Investigation of *Rd* on Nusselt number.

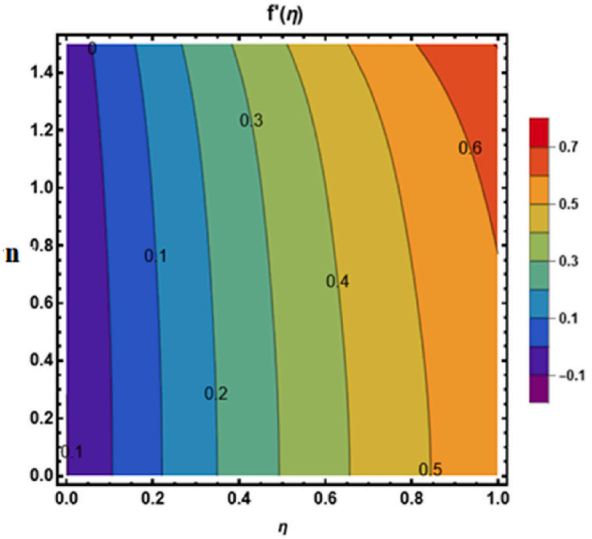

Fig. 6(a). Contour draw of viscosity constraint *n* versus speed outline.

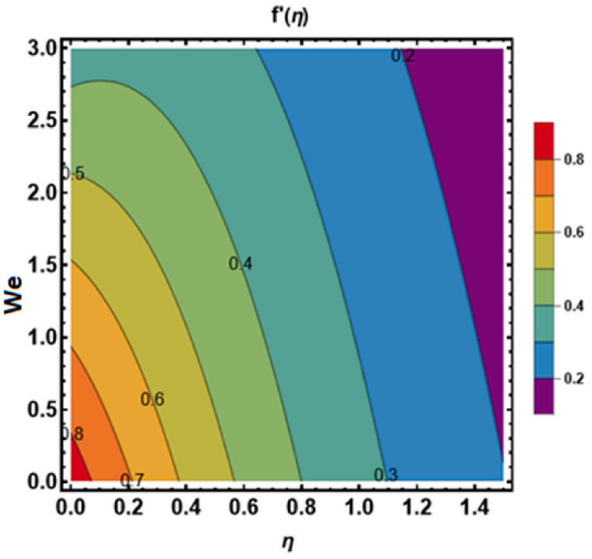

Fig. 6(b). Contour draw of dimensionless variable *We* versus rapidity outline.

illustrates the contour affect that the Prandtl number has on the temperature description. When new estimates of the Prandtl number are added, it is possible to see that the temperature distributions move in the opposite direction of the increase.

7. Tabular representation of sundry parameters impact on the drag coefficient and heat transfer nusselt number

Table 3 is designed to reflect the impact of sundry parameters on the drag coefficient along $x-$ axis and $y-$ axis respectively. From obtained numerical outcomes it is observed that the drag coefficient amplifies more along $x-$ axis contrast to $y-$ axis owing to an incremental change in M and n but diminishes in the case of remaining parameters like We, ω, and S. From Table 4 it is found that heat transference capacity improves in the case of amplification in M, S, ε, θ_w and R_H but diminishes in the case of remaining parameters like We, Pr, Sc, and n. From Table 5 it is clear that the heat transfer rate amplifies more in the case of tetra hybrid nanofluid TETHF in contrast to ternary hybrid nanofluid THNF. The ability of fluid to conduct heat amplifies in the case of TETHF in contrast to THNF which is stored by the PV panel and transfers more for offshore oil drilling purposes. From Table 6 it is observed that thermal radiation Rd plays a vital role in heat transfer rate. Nonlinear-based radiation has tremendous utilization in the industry like combustion reactors, polymer production, cleaning of medical tools, artificial satellites, etc. The overall temperature storage capacity of the PV panel amplifies in the case of Rd.

8. Validity

Table 7 displays the comparison analysis of obtained results due to an improvement in Pr in the case of heat transfer rate by keeping other parameters $We = 0, n = 1, A_1 = A_2 = 1$. The obtained outcomes are quite reliable and authentic when compared with the results achieved by Khan et al. [51] has taken.

9. Final remarks

The present article is designed to study the effect of the autocatalytic chemical reaction and variable thermal on inclined magnetized cross tetrahybrid moving subjected to a n expandable sheet. Nonlinear thermal radiation is considered in order to investigate and elevate the heat transfer effect. Cost analysis in terms of solar PV panel efficiency in contrast to diesel for oil drilling in the scenario of Pakistan has never been studied yet in the available literature. A novel tetrahybrid Xue nanofluid model (comprises of four different types of nanoparticles) has been developed and implemented. Comparison of the proposed novel nanofluid model with already existing models like ternary hybrid nanofluids and dihybrid nanofluid modes have been taken in this study. The final remarks and gist of the study are explained pointwise as under.

i. Solar energy is the kind of renewable energy best for countries like Pakistan, India, and Srilanka where the temperature rises above 40 Celcius in summer and the duration of sunset is about 16 h.
ii. Homogenous reaction physically describes the movement of nanoparticles within the fluid and due to immersing these nanoparticles temperature gets high for pseudo-plasticity and dilatant status.
iii. Numerical growth in the strength coefficient homogenous reaction parameter causes the decrement in the concentration file.
iv. Velocity becomes slow when magnetic strength becomes stronger because a stronger magnetic field produces Lorentz force, and it acts as an opposing force during the flow.

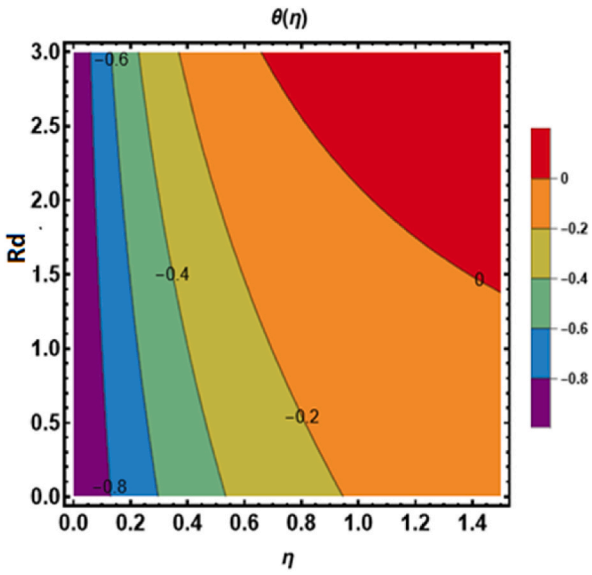

Fig. 6(c). Contour draw of variable Rd versus temperature outline.

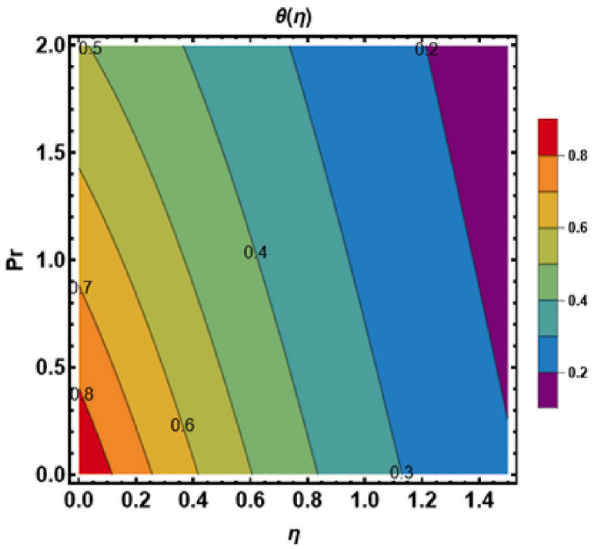

Fig. 6(d). Contour plot of parameter *Pr* against temperature field.

Table 3
Implication of on skin friction along $x-$ axis and $y-$ axis.

We	ω	*S*	*M*	*n*	Frictional force along $x-$ axis	Frictional force along $y-$ axis
0.1					1.4234	1.2700
0.2					1.2824	1.1703
0.3					1.1463	1.0817
0.5	0.2				0.9144	0.8110
	0.5				0.9135	0.7851
	0.7				0.9130	0.8214
		0.2			1.3601	1.1576
		0.4			1.3426	1.0213
		0.8			1.2022	0.9576
			0.4		1.3964	0.9344
			0.8		1.4810	0.9847
			1.2		1.5573	1.0945
				0.6	1.2853	0.9205
				0.8	1.4739	1.1979
				1.0	1.6391	1.3546

v. Velocity profile increases for enlarging cross fluid viscosity index parameter *n*.
vi. Diffusion is the transfer of molecules from a lower concentration to a higher concentration due to this temperature increase.
vii. It is concluded that greater *Pr* reduces the temperature of Carreau nanofluid for pseudo-plasticity and dilatant situations.
viii. Greater amount of thermal radiation gives a larger temperature which is stored by PV sheets and later used for drilling and navigational purposes on the offshore oil rig.
ix. More heat is produced, and the heat transfer production phenomenon amplifies in the case of TETHNF in contrast to THNF and HNF.
x. Parameters like *Rd*, θ_w, ε, R_H and TETHNF is the major factor responsible for amplification in heat generation which is stored by PV panel and used for various operations on the rig station.
xi. Using solar electricity at oil rigs could be expensive at first, yet it often ends up being less expensive than using diesel.
xii. 49% computational cost is reduced in the case of solar-powered energy as a replacement for diesel energy.

Author contribution statement

Tanveer Sajid, Wasim Jamshed formulated the problem. Wasim Jamshed and Mohamed R. Eid solved the problem. Tanveer Sajid, Wasim Jamshed, Salem Algarni, Talal Alqahtani, Mohamed R. Eid, Kashif Irshad, Gilder Cieza Altamirano, Sayed M El Din and Khadiga Wadi Nahar Tajer

Computed and scrutinized the results. All the authors equally contributed in writing and proof reading of the paper. All authors reviewed the manuscript.

Table 4
Effect of *Pr*, *Sc*, *We*, *S* and *n* on Nusselt number.

Pr	*Sc*	*M*	*We*	*S*	*n*	ε	θ_w	R_H	Nusselt Number
0.1									2.1319
0.2									1.9876
0.3									1.6523
0.5	0.3								1.7856
	0.6								1.5012
	0.9								1.2063
		0.7							1.1723
		0.9							1.5876
		1.1							2.0156
			0.7						2.2215
			0.9						2.0146
			1.1						1.8074
				0.7					1.5214
				0.9					1.8723
				1.2					1.9576
					0.4				1.6523
					0.7				1.4207
					1.1				1.2245
						1.0			3.0156
						1.5			3.2051
						2.0			3.4276
							1.0		2.5791
							1.5		2.9560
							2.0		3.2189
								1.0	1.7175
								1.5	2.0152
								2.0	2.4215

Table 5
The dimensionless Nusselt number against distinct parameters in the case of an increment in volume fraction of nanoparticles in the case of the Xue tetrahybrid nanofluid model.

Volume fraction of nanoparticles	Xue tetrahybrid nanofluid model	Volume fraction of nanoparticles	Xue tetrahybrid nanofluid model
$\phi = \phi_1 + \phi_2 + \phi_3$	$\frac{-1}{Nu_x Re_x^{\frac{-1}{2}}}$	$\phi = \phi_1 + \phi_2 + \phi_3 + \phi_4$	$\frac{-1}{Nu_x Re_x^{\frac{-1}{2}}}$
0.070	2.7632	0.10	3.5213
0.075	2.9135	0.11	3.8621
0.090	3.4152	0.12	4.1213
0.081	3.6901	0.13	4.3216

Table 6
Change in Nusselt number in the presence/absence of *Rd*.

Parameter	Absence of *Rd*	Presence of *Rd*
Rd	$\frac{-1}{Nu_x Re_x^{\frac{-1}{2}}}$	$\frac{-1}{Nu_x Re_x^{\frac{-1}{2}}}$
0.5	2.0152	3.4276
1	2.240	3.7822
1.5	2.6165	4.1428
2	2.8085	4.4212

Table 7
Comparison of the obtained results in the case of Nusselt number.

Parameter	Nusselt number	
Pr	Khan et al. [51]	Current Results
7	1.80433	1.80400
20	3.25603	3.25500
70	6.36662	6.36590

Declaration of competing interest

The authors declare that they have no known competing financial interests or personal relationships that could have appeared to influence the work reported in this paper.

Data availability

Data will be made available on request.

Acknowledgements

The authors extend their appreciation to the Deanship of Scientific Research at King Khalid University for funding this work through large group Research Project under grant number **RGP2/168/44**.

Nomenclature

n	Carreau fluid index
B_0	strength of magnetic field
k	thermal conductivity
τ	
C	
T	liquid temperature
D_A	Diffusion coefficient of chemical species A
D_B	Diffusion coefficient of chemical species B
T_∞	infinite temperature
T_f	
ω	angle of inclined magnetic field
ρ_f	fluid density
γ	
α	thermal diffusivity
C_p	specific heat
M	magnetic variable
Q^*	
Q	
χ	
E, F	autocatalysis
G_a, G_b	concentricity of chemical reactions
k_1, k_s	homo/heterogeneous reactions rate
ΔH_h	homogeneous heat reaction
BLMS	Backpropagated Levenberg- Marquard scheme
G_A	heterogeneous reaction stoichiometric coefficient
u, v, w	velocity component
x, y, z	space coordinates
σ^*, k^*	Stefan Boltzmann constant
Pr	Prandtl number
Nb	
Nt	
Sc	Schmidt number
We	local Weissenberg number
Bi	
u_w, v_w	stretchable rapidities
Rd	radiation parameter
υ	kinematic viscosity
C_f	skin-friction coefficient
Nu_x	Nusselt number
Re_x	local Reynold number
σ_1	
λ	
Δ	chemical reaction constant
ε	diffusion coefficient
R_H	homogenous reaction

f, g dimensionless velocities
K_T
MODU Mobile offshore digging unit

References

[1] W. Jamshed, M.R. Eid, A. Aissa, A. Mourad, K.S. Nisar, F. Shahzad, C.A. Saleel, V. Vijayakumar, Partial velocity slip effect on working magneto non-Newtonian nanofluids flow in solar collectors subject to change viscosity and thermal conductivity with temperature, PLoS One 16 (2021), e0259881.
[2] M.R. Eid, F. Mabood, Two-phase permeable non-Newtonian cross-nanomaterial flow with Arrhenius energy and entropy generation: Darcy-Forchheimer model, Phys. Scripta 95 (2020), 105209.
[3] P.J. Carreau, Rheological equations from molecular network theories, Trans. Soc. Rheol. 16 (1) (1972) 99–127.
[4] Z. Sabir, A. Ayub, J.L. Guirao, S. Bhatti, S.Z.H. Shah, The effects of activation energy and thermophoretic diffusion of nanoparticles on steady micropolar fluid along with Brownian motion, Adv. Mater. Sci. Eng. 2020 (2020), 2010568.
[5] A. Ayub, H.A. Wahab, S.Z. Shah, S.L. Shah, A. Darvesh, A. Haider, Z. Sabir, Interpretation of infinite shear rate viscosity and a nonuniform heat sink/source on a 3D radiative cross nanofluid with buoyancy assisting/opposing flow, Heat Transf 50 (5) (2021) 4192–4232.
[6] A. Ayub, H.A. Wahab, Z. Sabir, A. Arbi, A note on heat transport with aspect of magnetic dipole and higher order chemical process for steady micropolar fluid, in: Computational Overview of Fluid Structure Interaction Book, vol. 97, Intech. Open, 2020.
[7] S.Z.H. Shah, A. Ayub, Z. Sabir, W. Adel, N.A. Shah, S.J. Yook, Insight into the dynamics of time-dependent cross nanofluid on a melting surface subject to cubic autocatalysis, Case Stud. Therm. Eng. 27 (2021), 101227.
[8] H.A. Wahab, S.Z.H. Shah, A. Ayub, Z. Sabir, M. Bilal, G.C. Altamirano, Multiple characteristics of three-dimensional radiative Cross fluid with velocity slip and inclined magnetic field over a stretching sheet, Heat Transf 50 (4) (2021) 3325–3341.
[9] A. Ayub, Z. Sabir, G.C. Altamirano, R. Sadat, M.R. Ali, Characteristics of melting heat transport of blood with time-dependent cross-nanofluid model using Keller–Box and BVP4C method, Eng. Comput. 38 (4) (2022) 3705–3719.
[10] A. Ayub, Z. Sabir, D.N. Le, A.A. Aly, Nanoscale heat and mass transport of magnetized 3-D chemically radiative hybrid nanofluid with orthogonal/inclined magnetic field along rotating sheet, Case Stud. Therm. Eng. 26 (2021), 101193.
[11] S.Z. Shah, H.A. Wahab, A. Ayub, Z. Sabir, A. haider, S.L. Shah, Higher order chemical process with heat transport of magnetized cross nanofluid over wedge geometry, Heat Transfer 50 (4) (2021) 3196–3219.
[12] A. Ayub, A. Darvesh, G.C. Altamirano, Z. Sabir, Nanoscale energy transport of inclined magnetized 3D hybrid nanofluid with Lobatto IIIA scheme, Heat Transf 50 (7) (2021) 6465–6490.
[13] A. Ayub, H.A. Wahab, S.Z.H. Shah, S.L. Shah, Z. Sabir, S. Bhatti, On heated surface transport of heat bearing thermal radiation and MHD Cross flow with effects of nonuniform heat sink/source and buoyancy opposing/assisting flow, Heat Transf 50 (6) (2021) 6110–6128.
[14] K. Hosseinzadeh, S. Roghani, A.R. Mogharrebi, A. Asadi, M. Waqas, D.D. Ganji, Investigation of cross-fluid flow containing motile gyrotactic microorganisms and nanoparticles over a three-dimensional cylinder, Alex. Eng. J. 59 (5) (2020) 3297–3307.
[15] T. Hayat, M.I. Khan, M. Tamoor, M. Waqas, A. Alsaedi, Numerical simulation of heat transfer in MHD stagnation point flow of Cross fluid model towards a stretched surface, Results Phys. 7 (2017) 1824–1827.
[16] M. Waqas, Simulation of revised nanofluid model in the stagnation region of cross fluid by expanding-contracting cylinder, Int. J. Numer. Methods Heat Fluid Flow 30 (2020) 2193–2205.
[17] F. Sultan, W.A. Khan, M. Ali, M. Shahzad, M. Irfan, M. Khan, Theoretical aspects of thermophoresis and Brownian motion for three-dimensional flow of the cross fluid with activation energy, Pramana 92 (2) (2019) 1–10.
[18] S. Shaw, S.S. Samantaray, A. Misra, M.K. Nayak, O.D. Makinde, Hydromagnetic flow and thermal interpretations of Cross hybrid nanofluid influenced by linear, nonlinear and quadratic thermal radiations for any Prandtl number, Int. Commun. Heat Mass Tran. 130 (2022), 105816.
[19] H. Adun, D. Kavaz, M. Dagbasi, Review of ternary hybrid nanofluid: synthesis, stability, thermophysical properties, heat transfer applications, and environmental effects, J. Clean. Prod. 328 (2021), 129525.
[20] K.N. Sneha, G.P. Vanitha, U.S. Mahabaleshwar, D. Laroze, Effect of couple stress and mass transpiration on ternary hybrid nanoliquid over a stretching/shrinking sheet with heat transfer, Micromachines 13 (2022) 1694.
[21] J.S. Goud, P. Srilatha, R.S.V. Kumar, K.T. Kumar, U. Khan, Z. Raizah, H.S. Gill, A.M. Galal, Role of ternary hybrid nanofluid in the thermal distribution of a dovetail fin with the internal generation of heat, Case Stud. Therm. Eng. 35 (2022), 102113.
[22] S. Nasir, S. Sirisubtawee, P. Juntharee, A.S. Berrouk, S. Mukhtar, T. Gul, Heat transport study of ternary hybrid nanofluid flow under magnetic dipole together with nonlinear thermal radiation, Appl. Nanosci. 12 (9) (2022) 2777–2788.
[23] W. Cao, I. Animasaun, S.-J. Yook, V. Oladipupo, X. Ji, Simulation of the dynamics of colloidal mixture of water with various nanoparticles at different levels of partial slip: ternary-hybrid nanofluid, Int. Commun. Heat Mass Tran. 135 (2022), 106069.
[24] Z. Mahmood, Z. Iqbal, M.A. Alyami, B. Alqahtani, M.F. Yassen, U. Khan, Influence of suction and heat source on MHD stagnation point flow of ternary hybrid nanofluid over convectively heated stretching/shrinking cylinder, Adv. Mech. Eng. 19 (9) (2022).
[25] S.G. Krishna, M. Shanmugapriya, R. Sundareswaran, P.S. Kumar, MANFIS Approach for Predicting Heat and Mass Transport of Bio-Magnetic Ternary Hybrid Nanofluid Using Cu/Al2O3/MWCNT Nanoadditives, Biomass Conversion and Biorefinery, 2022, pp. 1–16.
[26] T. Sajid, A. Ayub, S.Z.H. Shah, W. Jamshed, M.R. Eid, E.S.M.T. El Din, R. Irfan, S.M. Hussain, Trace of chemical reactions accompanied with arrhenius energy on ternary hybridity nanofluid past a wedge, Symmetry 14 (2022) 1850.
[27] T. Sajid, W. Jamshed, M.R. Eid, G.C. Altamirano, F. Aslam, A.M. Alanzi, A. Abd-Elmonem, Magnetized Cross tetra hybrid nanofluid passed a stenosed artery with nonuniform heat source (sink) and thermal radiation: novel tetra hybrid Tiwari and Das nanofluid model, J. Magn. Magn Mater. 569 (2023), 170443.
[28] T. Sajid, W. Jamshed, R.W. Ibrahim, M.R. Eid, A. Abd-Elmonem, M. Arshad, Quadratic regression analysis for nonlinear heat source/sink and mathematical Fourier heat law influences on Reiner-Philippoff hybrid nanofluid flow applying Galerkin finite element method, J. Magn. Magn Mater. 568 (2023), 170383.
[29] Nilankush Acharya, Magnetized hybrid nanofluid flow within a cube fitted with circular cylinder and its different thermal boundary conditions, J. Magn. Magn Mater. 564 (2022), 170167.
[30] Nilankush Acharya, Ali J. Chamkha, On the magnetohydrodynamic Al2O3-water nanofluid flow through parallel fins enclosed inside a partially heated hexagonal cavity, Int. Commun. Heat Mass Tran. 132 (2022), 105885.
[31] N. Acharya, S. Maity, P.K. Kundu, Entropy generation optimization of unsteady radiative hybrid nanofluid flow over a slippery spinning disk, Proc. IME C J. Mech. Eng. Sci. 236 (11) (2022) 6007–6024.
[32] Nilankush Acharya, On the magnetohydrodynamic natural convective alumina nanofluidic transport inside a triangular enclosure fitted with fins, J. Indian Chem. Soc. 99 (2022), 100784.
[33] H.J. Xu, Z.B. Xing, F.Q. Wang, Z.M. Cheng, Review on heat conduction, heat convection, thermal radiation and phase change heat transfer of nanofluids in porous media: fundamentals and applications, Chem. Eng. Sci. 195 (2019) 462–483.
[34] A. Wakif, A. Chamkha, T. Thumma, I.L. Animasaun, R. Sehaqui, Thermal radiation and surface roughness effects on the thermo-magneto-hydrodynamic stability of alumina–copper oxide hybrid nanofluids utilizing the generalized Buongiorno's nanofluid model, J. Therm. Anal. Calorim. 143 (2) (2021) 1201–1220.
[35] J. Chen, C.Y. Zhao, B.X. Wang, Effect of nanoparticle aggregation on the thermal radiation properties of nanofluids: an experimental and theoretical study, Int. J. Heat Mass Tran. 154 (2020), 119690.

[36] P. Agrawal, P.K. Dadheech, R.N. Jat, K.S. Nisar, M. Bohra, S.D. Purohit, Magneto Marangoni flow of γ− Al_2O_3 nanofluids with thermal radiation and heat source/sink effects over a stretching surface embedded in porous medium, Case Stud. Therm. Eng. 23 (2021), 100802.
[37] J. Prakash, E.P. Siva, D. Tripathi, S. Kuharat, O.A. Bég, Peristaltic pumping of magnetic nanofluids with thermal radiation and temperature-dependent viscosity effects: modelling a solar magneto-biomimetic nanopump, Renew. Energy 133 (2019) 1308–1326.
[38] S.A. Khan, B. Ali, C. Eze, K.T. Lau, L. Ali, J. Chen, J. Zhao, Magnetic dipole and thermal radiation impacts on stagnation point flow of micropolar based nanofluids over a vertically stretching sheet: finite element approach, Processes 9 (7) (2021) 1089.
[39] L. Ali, B. Ali, X. Liu, T. Iqbal, R.M. Zulqarnain, M. Javid, A comparative study of unsteady MHD Falkner–Skan wedge flow for non-Newtonian nanofluids considering thermal radiation and activation energy, Chin. J. Phys. 77 (2022) 1625–1638.
[40] S. Shaw, S.S. Samantaray, A. Misra, M.K. Nayak, O.D. Makinde, Hydromagnetic flow and thermal interpretations of Cross hybrid nanofluid influenced by linear, nonlinear and quadratic thermal radiations for any Prandtl number, Int. Commun. Heat Mass Tran. 130 (2022), 105816.
[41] Nilankush Acharya, On the hydrothermal behavior and entropy analysis of buoyancy driven magnetohydrodynamic hybrid nanofluid flow within an octagonal enclosure fitted with fins: application to thermal energy storage, J. Energy Storage 53 (2022), 105198.
[42] Nilankush Acharya, Buoyancy driven magnetohydrodynamic hybrid nanofluid flow within a circular enclosure fitted with fins, Int. Commun. Heat Mass Tran. 133 (2022), 105980.
[43] M.R. Eid, K. Mahny, A.F. Al-Hossainy, Homogeneous-heterogeneous catalysis on electromagnetic radiative Prandtl fluid flow: Darcy-Forchheimer substance scheme, Surface. Interfac. 24 (2021), 101119.
[44] T.H. Alarabi, A.M. Rashad, A. Mahdy, Homogeneous–heterogeneous chemical reactions of radiation hybrid nanofluid flow on a cylinder with Joule heating: nanoparticles shape impact, Coatings 11 (2021) 1490.
[45] M.I. Khan, S.A. Khan, T. Hayat, S. Qayyum, A. Alsaedi, Entropy generation analysis in MHD flow of viscous fluid by a curved stretching surface with cubic autocatalysis chemical reaction, Eur. Phys. J. A 135 (2) (2020) 1–17.
[46] M. Waqas, A mathematical and computational framework for heat transfer analysis of ferromagnetic non-Newtonian liquid subjected to heterogeneous and homogeneous reactions, J. Magn. Magn Mater. 493 (2020), 165646.
[47] U. Ali, M.Y. Malik, K.U. Rehman, M.S. Alqarni, Exploration of cubic autocatalysis and thermal relaxation in a non-Newtonian flow field with MHD effects, Physica A549 (2020), 124349.
[48] Y.M. Chu, M.I. Khan, M.I. Ur Rehman, S. Kadry, M.K. Nayak, Flow and thermal management of MHD Cross nanofluids over a thin needle with auto catalysis chemical reactions, Int. J. Mod. Phys. E B34 (30) (2020), 2050287.
[49] https://www.globalpetrolprices.com/Pakistan/diesel_prices.
[50] https://www.solarreviews.com/solar-panel-cost.
[51] M. Khan, Manzur mehwish, rahman masood ur, boundary-layer flow and heat transfer of cross fluid over a stretching sheet, Therm. Sci. 23 (2019) 307–318.